Master's Thesis

Characterization of the auxiliary activity enzymes *Trichoderma reesei* TrAA3_2, TrAA9A and *Podospora anserina* PaAA9E, with potential roles in cellulose modification

Mimmu Hiltunen

University of Jyväskylä

Department of Biological and Environmental Science

Cell and Molecular Biology

16 April 2021

UNIVERSITY OF JYVÄSKYLÄ, Faculty of Mathematics and Science
Department of Biological and Environmental Science
Cell and Molecular Biology

Mimmu Hiltunen: Characterization of the auxiliary activity enzymes *Trichoderma reesei* TrAA3_2, TrAA9A and *Podospora anserina* PaAA9E, with potential roles in cellulose modification

MSc thesis: 46 p., 0 appendices
Supervisors: Senior scientist Martina Andberg and professor Jari Ylänne
Reviewers: PhD Tatu Haataja and professor Perttu Permi
April 2021

Keywords: biofuels, biomaterials, lignocellulose, lytic polysaccharide monooxygenase

Sustainably produced fuels and materials will be critical for the survival of our species, but a cost and time efficient production method is yet to be developed. Plant-based waste could be a part of the solution: one of its main components, cellulose, is a starting point for the production of biofuels and chemicals. However, the recalcitrant nature of the main component of plant-based waste, lignocellulose, as well as the enigmatic nature of lignocellulolytic enzymes and their cooperation, has hindered adopting applications on a global scale. The aim of this study was to characterise three fungal enzymes with potential roles in lignocellulose degradation. First, we aimed to characterise the activity and phylogenetic location, as well as build a homology model, of a novel Trichoderma reesei AA3_2 subfamily enzyme (TrAA3_2). Secondly, we aimed to characterise the H_2O_2 dependency as well as thermal and pH stability of two lytic polysaccharide monooxygenases (TrAA9A and PaAA9E). Thirdly, we aimed to evaluate the effects of TrAA3_2, TrAA9A, and PaAA9E on the hydrolysis of spruce biomass by a cellulase mixture. We found that TrAA3_2 is phylogenetically closest to glucose oxidases but were unable to detect activity with any of the assayed carbohydrate or alcohol substrates. The homology model revealed that the substrate-binding residues of TrAA3_2 differ from those found in two well-characterised oxidative glucose active enzymes, possibly explaining the apparent inactivity for glucose. Furthermore, we found both

TrAA9A and PaAA9E to be active with both O_2 and H_2O_2 as a cosubstrate, and to be stable at 40 °C and pH 5–7. TrAA9A was found to enhance the hydrolytic efficiency of a cellulase cocktail mimicking commercial lignocellulolytic cocktails. Based on our results, TrAA9A and PaAA9A display both oxidase and peroxidase activity, and may be good candidates for practical applications.

JYVÄSKYLÄN YLIOPISTO, Matemaattis-luonnontieteellinen tiedekunta
Bio- ja ympäristötieteiden laitos
Solu- ja molekyylobiologia

Mimmu Hiltunen:	Selluloosan muokkaukseen mahdollisesti osallistuvien avustavien entsyymien *Trichoderma reesei* TrAA3_2, TrAA9A ja *Podospora anserina* PaAA9E karakterisointi
Pro gradu -tutkielma:	46 s., 0 liitettä
Työn ohjaajat:	Vanhempi tutkija Martina Andberg ja professori Jari Ylänne
Tarkastajat:	FT Tatu Haataja ja professori Perttu Permi
Huhtikuu 2021	

Hakusanat: biomassa, biomateriaalit, lignoselluloosa, lyyttinen polysakkaridimono-oksygenaasi

Energian ja materiaalien tuotosta on tultava kestävän kehityksen periaatteiden mukaista, mikäli aiomme jatkaa nykyistä elämäntyyliämme. Kasvipohjaisen jätteen hyödyntämistä biopolttoaineiden ja kemikaalien valmistamisessa on pitkään harkittu vaihtoehtona uusiutumattomille lähtömateriaaleille, ja nykyteknologialla sen käsittely selluloosan vapauttamiseksi on mahdollista. Kuitenkin lignoselluloosa – kasvipohjaisen jätteen pääainesosa – on rakenteeltaan niin jäykkää, ettei sen hajottaminen suurella mittakaavalla ole vielä kannattavaa. Tässä projektissa tutkittiin kolmea lignoselluloosan hajottamiseen osallistuvaa entsyymiä, joista yksi on uusi AA3_2 –tyypin entsyymi (*Trichoderma reesei* TrAA3_2) ja kaksi ovat tunnettuja AA9 –perheen lyyttisiä polysakkaridimono-oksygenaaseja (*Trichoderma reesei* TrAA9A ja *Podospora anserina* PaAA9E). Tavoitteena oli ensiksi määrittää TrAA3_2:n substraatti ja elektroninvastaanottaja, sekä verrata sitä muihin saman perheen entsyymeihin fylogeneettisesti ja homologiamallin perusteella. Toiseksi, halusimme tutkia TrAA9A:n ja PaAA9E:n stabiilisuutta ja määrittää niiden aktiivisuuden riippuvuutta kuparista, sekä vetyperoksidista. TrAA3_2:lle ei havaittu aktiivisuutta yhdelläkään substraatti-elektroninvastaanottajaparilla. Fylogeneettisesti TrAA3_2 on lähimpänä glukoosioksidaaseja, mutta homologiarakenteen perusteella sen substraattia sitovat aminohapot eivät vastaa kahden tunnetun glukoosioksidaasin vastaavia aminohappoja, mikä voi osittain selittää miksei aktiivisuutta havaittu. Tulostemme perusteella sekä TrAA9A, että

PaAA9E voivat käyttää sekä happea, että vetyperoksidia kosubstraattina. Lisäksi molemmat ovat stabiileja pH välillä 5–7 ja 40 °C:ssa. Toisin kuin PaAA9E, TrAA9A parantaa tässä käytetyn sellulaasiseoksen hydrolyyttistä aktiivisuutta, mutta vetyperoksidin lisääminen TrAA9A-sellulaasi-reaktioon ei ennestään parantanut hydrolyysitehokkuutta. Näiden tulosten perusteella PaAA9A ja TrAA9A voisivat olla sopivia kandidaatteja käytännön sovelluksiin.

TABLE OF CONTENTS

TERMS AND ABBREVIATIONS

TERMS

Biomass	Organic material that can be used in energy production
Lignocellulose	The main component of plant cell walls

ABBREVIATIONS

AA	auxiliary activity
AAO	aryl-alcohol oxidase
CAZYme	carbohydrate-active enzyme
2,6-DMP	2,6-dimethoxyphenol
GDH	glucose dehydrogenase
GOx	glucose oxidase
LPMO	lytic polysaccharide monooxygenase
PDH	pyranose dehydrogenase
PaAA9E	*Podospora anserina* AA9E –family LPMO
SSN	sequence similarity network
TrAA9A	*Trichoderma reesei* AA9A –family LPMO

1 INTRODUCTION

Our current use of natural resources is unsustainable but employing alternative methods of energy and material production could help us continue to meet global energy demands while keeping the earth habitable. One alternative source for energy and material production is waste – particularly

plant-based waste - produced as a by-product of industrial and agricultural processes. Currently, however, plant-based waste is not used on a meaningful scale as a source material, mainly due to the cost and time span associated with its processing.

1.1 End Products of Plant-Biomass Processing

While the end products of processing plant-based biomass are not the focus of this study, a brief overview of some common end products is warranted to provide a contextual framework. Biofuels, fuels produced by the conversion of biomass, are commonly grouped into four generations based on the source material. First generation biofuels, which use starchy crops, vegetable oils and animal fats as source materials, are currently the most common biofuels (Zabed et al. 2019). However, using other sources is crucial as first-generation sources do not provide enough biofuel for the growing demand (Sankaran et al. 2019) and their use may threaten the food supply because the crops, oils, and fats are also fit for human consumption. Second generation biofuels are derived from waste biomass such as wood and agricultural residues (Zabed et al. 2019), whereas third generation biofuels originate from algae and fourth generation from genetically modified feedstock (Sankaran et al. 2019). Second, third, and fourth generation sources are all viable alternatives to first generation biofuels, but in this study the focus is on improving the processing of plant-based biomass. Synthetic plant-derived materials include products such as textiles, paper, and plastics, many of which can be produced from plant-based waste. For example, clothing and beverage bottles are often produced from polyethylene terephthalate (commonly known as PET), which can be produced from the components of plant cell walls (review Tuck et al. 2012). Another biodegradable plastic that can be produced from biomass is polylactic acid, which is used in packaging materials, fibres, and foams (review Tuck et al. 2012). Biomass can also be deconstructed to form traditional fibre products or nanocrystals, the latter of which is well suited for fabricating new materials, as well as stabilizing emulsions or hydrophobic drug particles. The preparation of these nanocelluloses does not require fully degrading biomass to glucose, but significant modification is necessary (Kontturi et al. 2018).

1.2 Lignocellulosic Biomass

Plant-based waste biomass – mostly composed of lignocellulose - is one of the source materials researchers are focusing on due to its abundance on earth (Guo et al 2018), and due to it posing no threat to the food supply, unlike conventional sources such as starchy crops. However, releasing glucose – a starting point for biofuel production - from lignocellulosic biomass is an extremely

complicated process and is yet to be perfected (Sankaran et al. 2019): Industrially extracting cellulose from lignocellulosic biomass is a multi-step process that involves severe heat or chemical pre-treatments, as well as enzymatic hydrolysis of polysaccharides.

Lignocellulose is a heterogeneous structure composed of lignin, hemicellulose, and cellulose and is a rigid structure that efficiently protects plant cells from microbial and enzymatic attack (Guo et al 2018). The first component of lignocellulose, lignin, is composed of cross-linked phenolic monomers, such as coniferyl, sinapyl, and coumaryl alcohol (Adler, 1977). The second component is hemicellulose, which is covalently linked to lignin. Hemicelluloses are β-(1→4) -linked polysaccharides, such as glucomannans, mannans, xylans, and xyloglucans (review by Scheller & Ulvskov, 2010). The third component, cellulose, is composed of D-glucose monomers linked via β-glycosidic bonds. Chains of D-glucose monomers additionally hydrogen bond to one another and can be organized into a crystalline structure. The elements of lignocellulose are intertwined with one another as a complex matrix: chains of hemicelluloses surround cellulose microfibrils and lignin fills gaps between the carbohydrate components. The structure of lignocellulose is further complicated by the variability of hemicellulose and lignin structures, as well as the crystalline regions of cellulose. Because all components of lignocellulose are interwined with one another it is necessary to break down both hemicellulose and lignin before it is possible to gain access to cellulose, which is the source material for many further applications (Champreda et al. 2019).

Some fungi can degrade or modify lignocellulose enzymatically under mild conditions, which makes them very interesting from the perspective of biotechnology, as their abilities can be enhanced and exploited in industrial applications (Cragg et al. 2015). Fungi use an array of enzymes to degrade lignocellulose: ligninases destroy the outer lignin layer, which gives another set of enzymes access to hemicellulose, and cellulases free glucose from the crystalline cellulose structure (Champreda et al. 2019). The essential cellulases for cellulose hydrolysis are endoglucanases (EC 3.2.1.4.), cellobiohydrolases (EC 2.3.1.91), and β-glucosidases (EC 3.2.1.21). Endoglucanases attack non-crystalline regions of cellulose and in this way uncover cellulose chain-ends, which can be attacked by other cellulases. Cellobiohydrolases act specifically on either reducing or non-reducing ends of crystalline cellulose and release cellobiose (dimer of glucose), which β-glucosidases can further hydrolyse to release glucose (Wang & Zhang, 2013). The cellulolytic system of *T. reesei* for example consists of several endoglucanases and two cellobiohydrolases, as well as auxiliary enzymes such as lytic polysaccharide monooxygenases (Figure 1, Karlsson 2002).

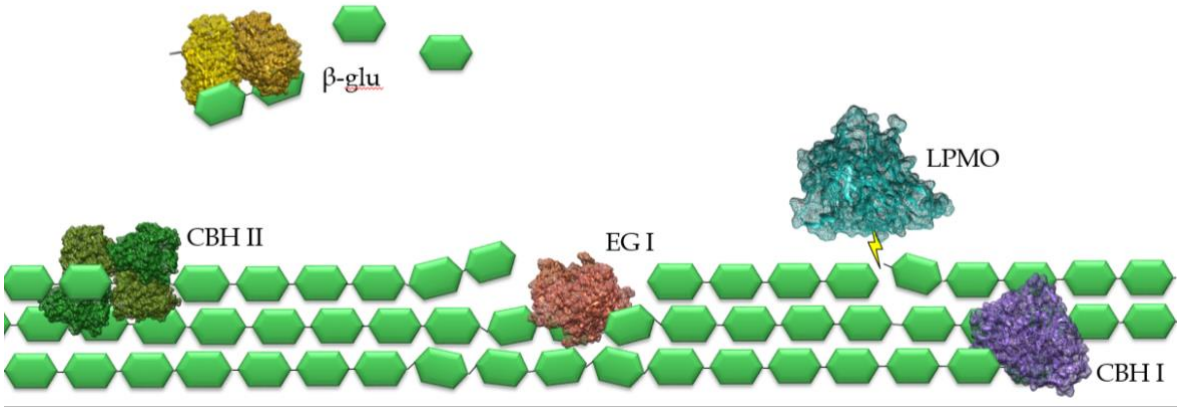

Figure 1 A representative cellulase system based on *T. reesei* system. Cellobiohydrolases I and II (**CBH I** and **II**) act on crystalline cellulose, endoglucanase I (**EG I**) on noncrystalline regions, and β-glucosidase (**β-glu**) on released oligomers. Lytic polysaccharide monooxygenase (**LPMO**) makes breaks in crystalline cellulose to make the chain accessible for CBH's.

In industrial biotechnology the cellulases mentioned above and other lignocellulolytic enzymes are combined to create a mixture referred to as an enzyme cocktail, which is used in further applications to degrade lignocellulose. However, due to the lack of fully characterised lignocellulolytic enzymes, the enzyme cocktails are not yet efficient enough in degrading lignocellulose to be employed on a global scale (Guo et al 2018).

1.3 Carbohydrate-Active Enzymes

The carbohydrate-active enzymes (CAZymes) classification system is a way of grouping the enzymes responsible for the breakdown and assembly of complex carbohydrates (Davies & Sinnott 2008) and is used to identify the enzymes in this study. In the CAZyme -system enzymes of the same family possess similar tertiary structures and catalytic mechanisms (Davies & Sinnott 2008) and all CAZymes are grouped hierarchically into superfamilies, families, and subfamilies (Figure 2). The critical cellulases described above (endoglucanases, cellobiohydrolases, and β –glucosidases) are part of the glycoside hydrolase superfamily, which consists of enzymes responsible for the hydrolysis of glycosidic linkages. In contrast, the enzymes studied in this project belong to the Auxiliary Activity (AA) superfamily, described as enzymes that aid other CAZymes in the degradation of plant cell walls by making the carbohydrates of the cell wall more accessible. More specifically, the enzymes studied here belong to the AA3 and AA9 families, which are defined as follows: AA3-family enzymes enhance lignocellulose degradation by cooperating with other AA-families, such as the AA9 family. The AA9 -family in turn consists of enzymes that cleave crystalline cellulose, thereby helping cellulases gain access to it (Lombard et al. 2013).

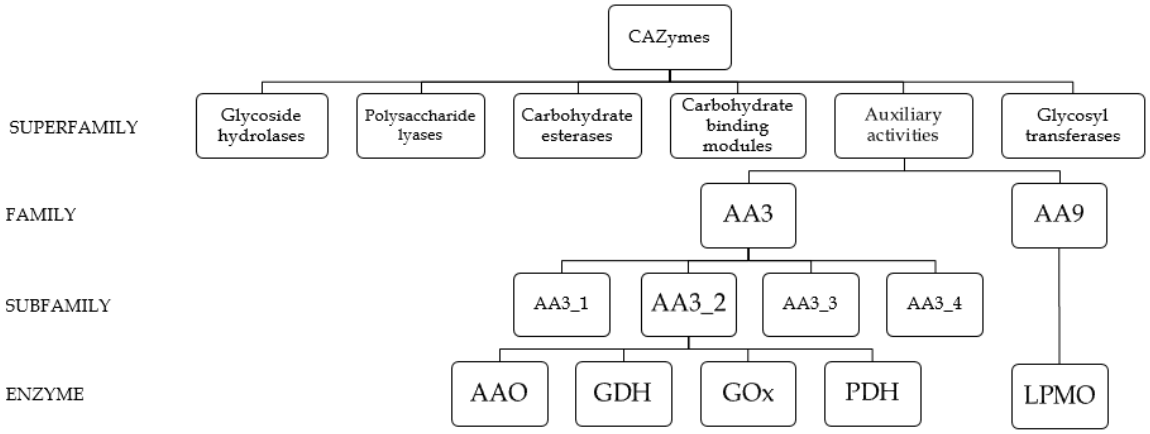

Figure 2 The hierarchy of CAZymes. CAZymes are ordered based on their primary sequence and function into super families, families, and subfamilies. The enzymes studied here belong to the Auxiliary activities superfamily families AA3_2 and AA9.

1.3.1 The AA3 Family

AA3s have various biological functions and are commonly found in wood-degrading fungi (Sützl et al. 2018), such as *T. reesei*. The primary function of AA3s is to assist other CAZymes by stimulating their catalytic activity and increasing the rate of lignocellulose degradation. AA3s depends on a flavin-adenine dinucleotide (FAD) cofactor for catalytic activity and exert their function through catalysing the oxidation of alcohols or carbohydrates to H_2O_2 and hydroquinones (Sützl et al. 2018). Lombard et al. (2013) group AA3s into four subfamilies from AA3_1 to AA3_4, of which only the AA3_2 subfamily enzymes are reviewed here (for further review see Lombard et al. 2013). The AA3_2 subfamily includes four types of enzymes: aryl-alcohol oxidoreductase (AAO, EC 1.1.3.7), glucose-1 oxidases (GOx, EC 1.1.3.4), glucose-1 dehydrogenases (GDH, EC 1.1.5.9), and pyranose dehydrogenases (PDH, EC 1.1.99.29).

As oxidoreductases, the AA3_2 enzymes all share some common features in their reaction mechanism (Lombard et al. 2013), and the general reactions catalysed by the subtypes are displayed in equations 1 (AAO) and 2 (GOx, GDH, and PDH). Both an electron donor and an electron acceptor are necessary for the function of the enzyme and therefore two reactions occur essentially simultaneously: the substrate is oxidised whilst the electron acceptor is reduced. The FAD cofactor mediates the reaction by being transiently reduced to $FADH_2$ by the substrate and is re-oxidised to FAD when the electron acceptor is reduced. The preferred electron donor and acceptor vary between enzyme types and impact the role and possible utility of the enzyme (Lombard et al. 2013).

$$benzyl\ alcohol + O_2 \rightarrow\ aldehyde +\ H_2O_2 \qquad (1)$$

$$saccharide + O_2 \rightarrow gluconolactone, aldonolactone\ or\ (di)ketosugar + H_2O_2 \quad (2)$$

AAOs are the most thoroughly characterised enzyme type of the AA3_2 subfamily. They catalyse the oxidation of primary alcohol groups (Sützl et al. 2018) and their proposed function is to provide H_2O_2 to peroxidases that degrade lignin (reviewed by Yann et al. 2016). AAO substrates are plentiful including both fungal and lignin derived aromatic and aliphatic polyunsaturated alcohols, but most characterised AAOs seem to prefer non-phenolic aromatic substrates, such as p-anisyl alcohol. The preferred electron acceptor of AAOs based on research so far appears to be O_2 (Sützl et al. 2018, Jeske et al. 2019).

GOx is another well-characterised AA3_2 enzyme type that is produced by some fungi and insects (Wong et al. 2008) and may have a natural role of acting as an antibacterial agent (Bucekova et al. 2014). Moreover, GOx's can reportedly aid fungi in lignin degradation (Ramasamy, Kelley & Redy 1985) and are used in biotechnology applications including textile bleaching (Tzanov et al. 2002) and artificial muscles (Mashayekhi Mazar et al. 2019). Other known subtypes of the AA3_2 subfamily are GDH and PDH. GDHs are very similar to GOx's both in their function and in structure, but they differ in the exact reaction mechanism as well as preferred electron acceptor: GOx's use O_2 while GDHs use quinones (Sützl et al. 2018). Fungal PDH's have not yet been characterised in detail, but their distinguishing features seem to be a preference for pyranose electron acceptors and a lax substrate specificity (Sützl et al. 2018). For example, a PDH from *Agaricus xanthoderma* is able to oxidise mono- and oligosaccharides, as well as glycosides (Kujawa et al. 2007).

1.3.2 The AA9 Family

The AA9 family consists of fungal lytic polysaccharide monooxygenases (LPMOs, formerly GH61 EC 1.14.99.54 and EC 1.14.99.56) which are copper dependent enzymes that cleave crystalline cellulose, thus making it more accessible to cellulases. The existence of LPMO –like, nonhydrolytic, enzymes was postulated decades ago (Reese et al. 1950) and their ability to increase the rate of chitin degradation (analogous to cellulose degradation) was demonstrated in the early 2000's (Vaaje-Kolstad et al. 2005) but their unusual oxidative reaction mechanism was not revealed until 2010 (Vaaje-Kolstad et al. 2010). Since then, the pace of LPMO research has only picked up as their important role in lignocellulose degradation becomes clearer.

Though LPMOs exert their helper function mainly by breaking bonds of crystalline cellulose, making it more accessible for cellulases, some have other substrates, including hemicellulose and

soluble glucose oligosaccharides (reviewed by Frommhagen et al. 2018). It is difficult to say with certainty what the substrate range is due to the size of this family and lack of characterised members: according to CAZY 29 AA9 LPMOs have been characterised and 17 structures solved so far (http://www.cazy.org/AA9.html).

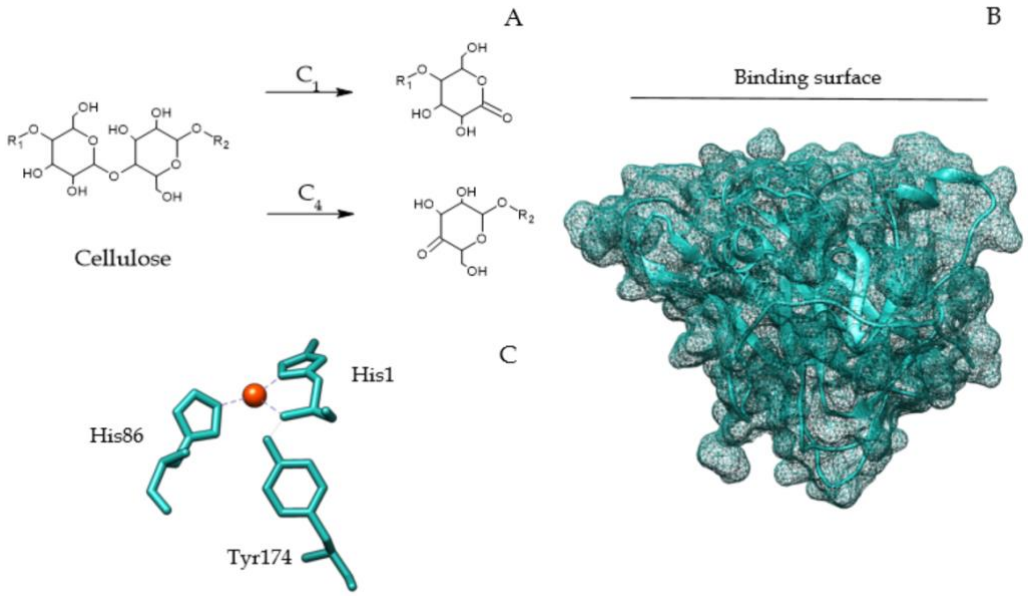

Figure 3 Features of LPMOs Modelled with *Hypocrea jecorina* AA9A (PDB ID: 502W) **(A)** LPMOs cleave cellulose by preferentially inserting an oxygen at either the C1, C4, or both. The characteristic features of LPMOs include is a flat binding surface **(B)** and a copper bound by a histidine brace **(C).** This figure was inspired by the depiction of LPMO features by Vaaje-Kolstad et al. (2010).

LPMOs are structurally diverse but have some characteristic features such as a flat active site surface (Figure 3 B) in with a histidine brace: two histidines and either a tyrosine or an alanine surrounding a surface-exposed copper (Figure 3 C). The flat active site surface and the exposed copper are unusual structural elements, but are well adapted for binding flat, crystalline substrates (reviewed by Bissaro et al. 2018). Some LPMOs are also bound to a non-catalytic carbohydrate binding protein module (found in the CBM superfamily in Figure 2) which may help the LPMO bind to its substrate. LPMOs oxidise cellulose selectively at either the C1, C4 or both (see Figure 3 A). It is still unclear what determines the preferred oxidation site, but distinct structural features such as the identity of the CBM, substrate, reductant, and the third copper-binding amino acid, may explain some of the selectivity (Danneels et al. 2019; reviewed by Frommhagen et al. 2018).

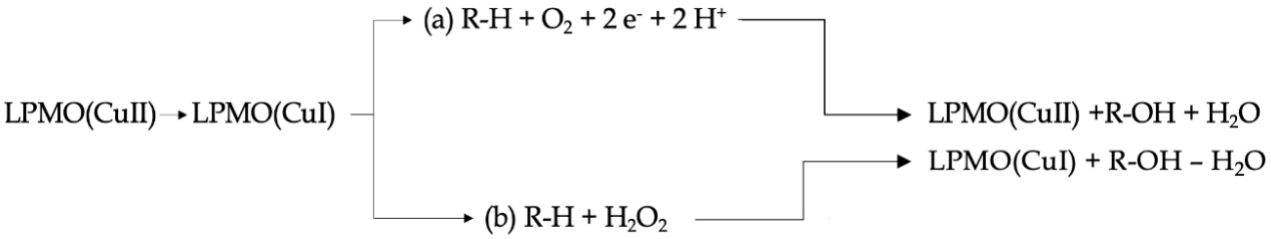

Figure 4 General LPMO reaction mechanism. First, the LPMO active site copper is reduced to Cu(I). Secondly either (a) O_2 or (b) H_2O_2 acts as a cosubstrate to hydrolyse crystalline cellulose (R-H) by converting the C1 or C4 ketone formed by the LPMO copper to a hydroxyl group (conversion not shown). In the reaction with O_2 as a cosubstrate, two additional electrons and protons are required, whereas H_2O_2 provides all necessary components to complete the cycle.

The activity of LPMOs begins with the reduction of its copper after which a cosubstrate - either O_2 or H_2O_2 - is necessary to complete the catalytic cycle (see Figure 4 for an overview). When O_2 acts as the cosubstrate, two additional protons and an electron have to be obtained from elsewhere, and the copper needs to be reduced at the beginning of each catalytic cycle. In contrast, H_2O_2 can provide all the necessary constituents to fuel the activity for several catalytic cycles and the copper remains in a reduced state. Even though both O_2 and H_2O_2 are able to drive the activity, the debate of the "true" LPMO cosubstrate is ongoing (review by Bissaro et al. 2018).

1.3.2.1. Connection between AA9 and AA3 -family enzymes

In fungal lignocellulolytic systems arrays of coexpressed enzymes work synergistically to degrade all parts of lignocellulose. While AA9 –family enzymes themselves promote the activity of cellulases, the activity of the LPMOs is enhanced by AA3-enzymes, most notably AA3_1 cellobiose dehydrogenase, which catalyses the oxidation of cellobiose to cellobiono-1,5-lactone (CDH, EC 1.1.99.18) (Phillips et al. 2011), which can directly transfer electrons to AA9 LPMOs or may do so via an H_2O_2 intermediate (review Bissaro et al. 2018). However, some fungi, like *T. reesei*, do not encode CDH. This raises the possibility of another CDH –like enzyme, possibly an AA3_2 enzyme, that may promote the activity of *T. reesei* LPMOs.

1.4 Podospora anserina and Trichoderma reesei

The filamentous ascomycete *T. reesei* was discovered 70 years ago and has one of the most powerful of characterised cellulolytic systems (reviewed by Bischof, Ramoni & Seiboth 2016). The cellulolytic

capabilities of *T. reesei* make it highly suitable for industrial biofuel applications (in 2016 around 80% of bioethanol was produced with *T. reesei* enzyme formulations). Despite its popularity in industrial applications, *T. reesei* encodes very few cellulases and hemicellulases compared to other lignocellulolytic fungi and is incapable of degrading lignin (Martinez et al. 2008).

Podospora anserina (*P. anserina)* has been steadily used in research and industry over a 100-year period because it has a short generation time and is easy to grow *in vitro*. The genome of *P. anserina* encodes a magnitude of enzymes involved in cellulose and xylan hydrolysis, as well as lignin breakdown (Espagne et al. 2008), which makes sense in light of its role in nature: *P. anserina* grows on herbivore dung, when most easily digestible carbon sources are absent (review by Silar 2013). *P. anserina* also encodes 33 LPMOs, which may have different functional roles: they can target different components of the plant cell wall and generate different oxidised/non-oxidised products (Bennati-Granier et al. 2015). In contrast to this, *T. reesei* only has two AA9 -LPMOs (Florencio et al. 2016). Interestingly, *P. anserina* and *T. reesei* may work synergistically in vitro as putative polysaccharide-degrading enzymes from *P. anserina* improve the hydrolysis of lignocellulosic biomass by *T. reesei* (Couturier et al. 2011).

1.5 Aim

In this study, the aim was to characterise three AA -enzymes. Firstly, we set to purify a novel *T. reesei* AA3_2 subfamily enzyme (TrAA3_2) and to characterize it e.g., for its substrate specificity, cofactor content and thermal stability. A homology model TrAA3_2 was to be built and compared to other AA3_2 structures, and a phylogenetic analysis to be conducted to see how TrAA3_2 relates to other AA3_2 subfamily members. Secondly, we wanted to assess the effect of copper loading and H_2O_2 on the activities of LPMOs from *P. anserina* (PaAA9E) and *T. reesei* (TrAA9A). Moreover, the thermal and pH stability of the two LPMOs was analysed. The practical application of these LPMOs and potential synergistic effects of TrAA3_2 and TrAA9A is investigated by performing a hydrolysis experiment.

2 MATERIALS AND METHODS

2.1 Materials

All chemicals were of the highest analytical grade from SIGMA, unless otherwise mentioned. 4-20% gradient SDS-PAGE gels were used (Criterion 12-20 %, Stain Free, Bio Rad). Vivaspin centrifugal concentrators with a MWCO of 5000 were used throughout to concentrate samples (Sartorius). PD-10 Desalting columns with Sephadex® G-25 Medium (Cytiva) were used to exchange sample buffers.

2.2 Methods

2.2.1 Production and purification of *Trichoderma reesei* TrAA3_2

T. reesei strain M2576 expressing the *T. reesei* AA3_2 protein was cultivated in 24-well plates for five days in 4% lactose, 2% spent grain extract, 100 mM PIPPS, with di-ammonium citrate at 28 ºC, 800 rpm (Infors Multitron Shaker). The *T. reesei* cultivation supernatant was filtered (0.2 µM PES Filter Unit, VWR Vacuum Filtration) and half of the sample was stored at +4 ºC, and the other half at -20 ºC.

Ion exchange (IEX) chromatography was used to purify TrAA3_2. The isoelectric point, i.e., the pH at which the net surface charge is neutral, was calculated from the protein sequence using the ProtParam tool (https://web.expasy.org/protparam/). The pI was used to estimate the pH at which the protein would bind to the IEX column. To ensure proper binding it was ensured that the pH and conductivity of both the sample and the equilibration buffer had similar values.

TrAA3_2 was purified with ion exchange chromatography at pH 7 using a 5 ml HiTrap® DEAE Fast Flow column and an ÄKTA™ chromatography system (GE Healthcare). Before purification, the column was washed with 2 column volumes (CV) 2 M NaCl, 5 CV 1 M NaOH, and 2 CV 2 M NaCl, and rinsed with distilled water in between each step. Before adding the sample, the column was equilibrated with the running buffer. The running buffer (A) was 10 mM Na-phosphate pH 7, and the elution buffer (B) 10 mM Na-phosphate pH 7, 1 M NaCl. The protein was eluted with a multistep linear gradient (see steps in Figure 5). Fractions containing TrAA3_2 were identified with SDS-PAGE pooled and concentrated using Vivaspin centrifugal concentrators (at +4 ºC, 4000 rpm using an

Eppendorf 5810R centrifuge). The buffer of the concentrated sample was exchanged to 20 mM Na-phosphate pH 6 using PD-10 columns and stored at +4 ºC.

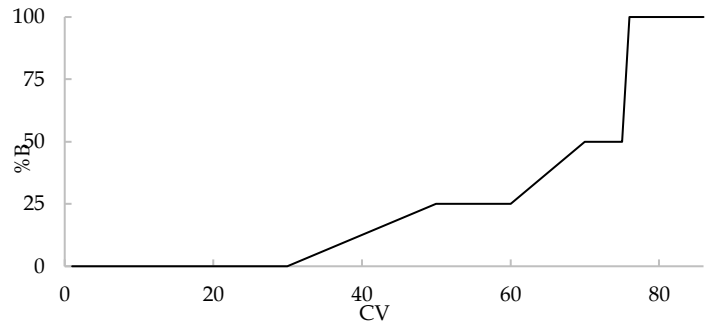

Figure 5 TrAA3_2 ion exchange chromatography purification steps plotted as %B against column volume. TrAA3_2 was purified with the ÄKTA chromatography system using a DEAE HiTrap column. The running buffer (A) was 10 mM Na-phosphate pH 7 and the elution buffer (B) was 10 mM Na-phosphate pH 7, 1 M NaCl. The column had been washed before the run. The sample was added at 5 CV, and any unbound protein was washed out with 25 CV buffer A. The bound sample was eluted by rising %B gradually first to 25, then 50, and finally 100.

2.2.2 Characterisation of *T. reesei* TrAA3_2

2.2.2.1 Spectral analysis of TrAA3_2 for secondary structure content and presence of FAD cofactor

Circular dichroism (CD) spectroscopy is a technique commonly used in molecular biology to obtain information about the native structure, apparent melting point, or ligand binding of a protein. The theoretical aspects of CD-spectroscopy are quite complex and beyond the scope of this study but briefly, a molecule is said to display circular dichroism if it absorbs left and right-handed circularly polarised light to different extents. CD-spectra are commonly plotted as degrees of ellipticity (calculated from the difference in intensity between left and right-handed light after passing through the sample) against the measured wavelength. Asymmetric (i.e., chiral) molecules, such as amino acids, have circular dichroism and their presence can thus be detected by CD-spectroscopy. Protein secondary structures – alpha-helices, β-sheets, and random coils - have characteristic spectra (represented in Figure 6). The characteristic alpha-helix spectrum has dips at 222 nm and 208 nm and a peak at 193 nm, whereas antiparallel β-sheets have a negative band at 218 nm and a positive band at 195 nm. The secondary structure content of a protein can be estimated directly from the CD-spectrum, and changes in the spectrum after for example heating the sample or adding a ligand provides information about how the secondary structure changes in response (Kelly & Price, 2005).

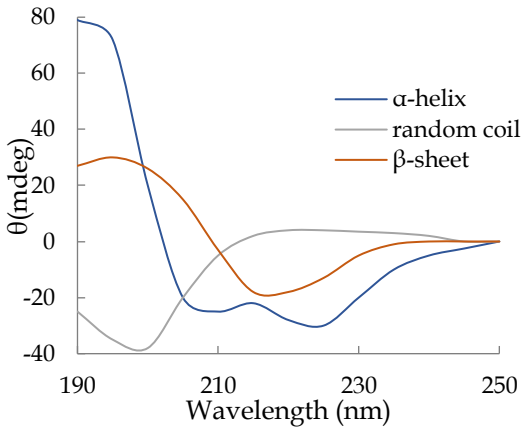

Figure 6 Characteristic CD-spectra of protein secondary structures.

The CD-spectra of 3 µM TrAA3_2 and 30 µM *Aspergillus niger* glucose oxidase (AnGOx) in 20 mM Na-phosphate pH 6 were measured at 25 ºC to observe the secondary structure content, then at 87 ºC to observe unfolding, and lastly again at 25 ºC to observe possible refolding of the protein. Measurements were made as duplicates in 1 nm steps, 1 s/point, between 240 and 195 nm using a bandwidth of 1 nm. During the measurements, the nitrogen flow was kept at 1 l/min. The samples were placed in a 1 mm cell (High Precision Cell, Quartz SUPRASIL QS, Hellma Analytics). All measurements were performed on a Chirascan spectrometer (Applied photophysics, UK) equipped with a Quantum Northwest TC125 heater, a Julabo AWC100 Air-to-Water Recirculating cooler, and a 150 W Xenon Arc lamp. The data was visualised and processed with the Pro-Data Viewer (v 4.1.9, Applied Photophysics) and Microsoft Excel.

The FAD –cofactor integrity of 14 µM TrAA3_2 and 8 µM AnGOx in 20 mM Na-phosphate pH 6 was evaluated by scanning the absorbance at 5 nm intervals between 600 and 250 nm using a Varioskan spectrophotometer (Thermo Electron Corporation).

2.2.2.2 TrAA3_2 activity assays

The activity of TrAA3_2 was measured with various assays using different substrates and electron acceptors.

2.2.2.2.1 Assays using O_2 as electron acceptor

The oxidase activity of AA3_2, i.e. using O_2 as electron acceptor, on various substrates can be monitored by coupling the production of hydrogen peroxide (H_2O_2) to a horseradish peroxidase

(HRP)-linked reaction. The produced H_2O_2 can then be detected in a photometric assay (HRP/2,2-azinobis(3-ethylbenzthiazoline)-6-sulfonic acid (ABTS)) at 418 nm.

Horseradish peroxidase (HRP) uses H_2O_2 to oxidise ABTS into a product detectable at 418 nm (see reaction 4). Because H_2O_2 is necessary for HRP activity, the reactions that generate it can be indirectly assayed by coupling them with the HRP-ABTS reaction. As some AA3_2 family enzymes are known to be oxidases, i.e., using O_2 as electron acceptor, their activity can be monitored by coupling their production of H_2O_2 to the HRP reaction (see reaction 1 & 2) The produced H_2O_2 can then be detected in a photometric assay (HRP (ABTS)).

$$D-glucose + O_2 \xrightarrow{AA3\_2} D-gluconolactone + H_2O_2 \quad (3)$$

$$H_2O_2 + \mathrm{ABTS} \rightarrow 2H_2O + \mathrm{ABTS_{ox}} \quad (4)$$

Here, 5 µM TrAA3_2 (buffer-exchanged supernatant in 0.1 M Na-phosphate pH 6) and 1-4 mM substrate (veratryl alcohol, L-arabinose, D-galactose, D-glucose, D-cellobiose, D-maltose, D-mannose, and D-xylose) was coupled with 2.5 mM ABTS and 10 µg/ml HRP in 0.1 M Na-phosphate pH 6. *Dactylium dendroides* galactose oxidase and *Aspergillus niger* glucose oxidase were used as positive controls. The change in absorbance at 418 nm was followed at RT for 15 min at 30 s intervals.

The ferric-xylenol orange (FOx) assay relies upon the reduction of Fe(II) to Fe(III) by a peroxide, and the binding of Fe(III) to xylenol orange, which can be detected at 560 nm (Gay et al. 1998, Viña-Gonzales et al. 2015). Here, the assay was used to see whether TrAA3_2 is able to reduce Fe(II) through the production of H_2O_2.by assaying 18 µg/ml TrAA3_2 (purified TrAA3_2 in 0.1 M Na-phosphate pH 6) with 10 mM veratryl alcohol and D-glucose

We also attempted to couple the activity of 7.2 µg/ml TrAA3_2 (purified TrAA3_2 diluted in 20 mM Na-phosphate pH 7) with TrAA9A by adding it to the 2,6-DMP assay detailed below in the context of LPMOs.

2.2.2.2.2 Assays with other electron acceptors

Some AA3_2 enzymes prefer quinoid electron acceptors to oxygen (see for example Kujawa et al. 2007; Mathieu et al. 2016) and therefore we assayed TrAA3_2 with two quinoid electron acceptors.

The decrease in absorbance at 600 nm can be detected when 2,6-dichlorophenolindophenol (DCIP) is reduced (see Figure 7). The assay is made more sensitive by adding phenazine methosulfate (PMS), which mediates the transfer of electrons (review by Bérénice et al. 2020). Here, we incubated 25 mM substrate (anisyl alcohol, cinnamyl alcohol, veratryl alcohol, L-arabinose, D-cellobiose, D-glucose, D-galactose, and D-maltose), 200 µM DCIP, and 100 µM PMS in 0.1 mM Na-phosphate pH 6 in a total volume of 75 µl for 10 min at RT before adding 25 µL TrAA3_2 buffer-exchanged supernatant in 0.1 M Na-phosphate pH 6) and following the absorbance at 600 nm for 60 min at 60 s intervals. *Caulobacter cresentus* aldose-aldose oxidoreductase was used as a positive control.

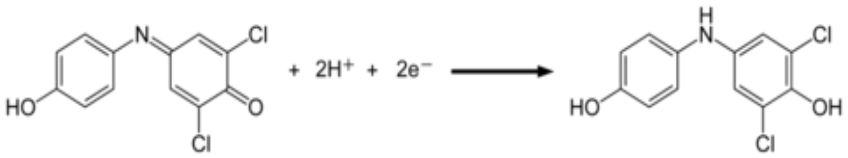

Figure 7 Reduction of DCIP by two protons and two electrons. DCIP is detectable spectrophotometrically at 600 nm, and its reduction can be followed by observing the decrease in absorbance at this wavelength.

Some AA3_2s are able to reduce p-benzoquinone (BQ) to hydroquinone, which produces a colorimetric response around 290 to 245 nm and it (Urban et al. 2006). Here, the activity of 20 µl in 200 µl TrAA3_2 (buffer-exchanged supernatant in 0.1 M Na-phosphate pH 6) was assayed with 100 µM BQ and 10 mM substrate (anisyl alcohol, cinnamyl alcohol, veratryl alcohol, D-glucose, and D-galactose) in 0.1 mM Na-phosphate pH 6 by following the absorbance at 290 nm for 20 min at 60 s intervals.

2.2.3 Phylogenetic analysis and homology modelling of TrAA3_2

A sequence similarity network (SSN) in which the most related proteins are grouped together, can be used to visualize relationships among protein sequences. An SSN was built as described by Sützl et al. (2019). Briefly, Sützl et al (2019) had identified 2439 AA3_2 family enzyme sequences, which could be divided to four phylogenetically distinct clusters that are roughly equivalent to the AA3_2 enzyme types (i.e., AAO, GDH, GOx, PDH). TrAA3_2 sequence was added to the sequences provided by Sützl et al. in order to analyse its phylogenetic relationship to other AA3_2 family enzymes. The SSN was generated using the online Enzyme Function Initiative–Enzyme Similarity Tool (EFI-EST, Zallot et al. 2019), where the alignment score cut-off (E-value) was set to 10^{-85},

corresponding to a sequence identity of 30%. The SSN was edited and visualised with Cytoscape (Shannon et al. 2003), where an organic layout was applied to the SSN. The SSN clusters were annotated based on the most common enzyme type in that cluster.

The primary amino acid sequence of TrAA3_2 (594 amino acids with the signal sequence) was used to build a 3D homology model of the TrAA3_2 enzyme with the SWISS-MODEL tool (Waterhouse et al. 2018), then visualised and analysed with UCSF Chimera (Pettersen et al. 2004).

2.2.4 Characterisation of *Trichoderma reesei* TrAA9A and *Podospora anserina* PaAA9E

2.2.4.1 Spectrophotometric LPMO assay using 2,6-DMP and H_2O_2

A spectrophotometric activity assay using 2,6-dimethoxyphenol (2,6-DMP) and H_2O_2, described by Breslmayr et al. (2018) to be a sensitive and reliable assay for LPMOs, is used throughout this study. The assay reaction is shown in reactions 3 and 4 below and consists of two key parts: (3) LPMO catalyses 2,6-DMP oxidation to two 2,6-DMP radicals. The radicals then dimerise non-enzymatically to form hydrocoerulignone (4) LPMO catalyses hydrocoerulignone oxidation to coerulignone, which can be detected at 469 nm.

$$2\ 2{,}6-\mathrm{DMP} + 1\ H_2O_2 \rightarrow 2\ 2{,}6-\mathrm{DMP\ radical} + 2\ H_2O \rightarrow 1\ \mathrm{hydrocoerulignone} \qquad (3)$$

$$1\ \mathrm{hydrocoerulignone} + H_2O_2 \rightarrow 1\ \mathrm{coerulignone} + 2\ H_2O \qquad (4)$$

2.2.4.2 Copper loading of TrAA9A and PaAA9E LPMOs

To test whether the activity of LPMOs can be improved, due to lack of copper in the enzyme, the purified TrAA9A and PaAA9E enzymes were loaded with a four-fold molar amount of copper sulphate ($CuSO_4$) in 20 mM Tris-HCl pH 8 for 30 min at RT. The excess copper was removed by PD-10 column and simultaneously exchanging the buffer to 25 mM Na-acetate pH 5. The molarity of purified TrAA9A and PaAA9E was determined by measuring the absorbance at 280 nm, using a theoretical extinction coefficient calculated by ProtParam (ε= 53 860 M^{-1} cm^{-1}, and 49 850 M^{-1} cm^{-1} for TrAA9A and PaAA9E, respectively) (http://au.expasy.org/tools/protparam.html). The activity of copper-loaded (+) and unloaded (-) enzymes was determined with the 2,6-DMP assay. The 2,6-DMP assay was performed by incubating 2,6-DMP with H_2O_2 in 20 mM Na-phosphate pH 8 (30 ºC, 300 rpm, 30 min) while TrAA9A (+/-) and PaAA9E(+/-) were diluted in 25 mM Na-phosphate pH 7. The reaction was started by adding the diluted enzymes into incubated mixtures, so that the

reactions contained 1.25 µM enzyme, 1 mM 2,6-DMP, 100 µM H_2O_2. The absorbance at 469 nm was followed at 30 s intervals for 20 min.

2.2.4.3 Thermal stability of TrAA9A and PaAA9E

The thermal stability of TrAA9A and PaAA9E was assessed by incubating 12.5 µM enzyme in 25 mM Na-phosphate pH 6 at 40, 60, and 70 ºC for 24 h, 6 h, 3 h, 30 min, 15 min, and 0 min before measuring enzyme activity with the 2,6-DMP assay described above. The buffer alone, as well as 12.5 µM $CuSO_4$ in buffer served as controls. The samples were incubated at RT for 15 min before assaying the activity to keep the assay temperature as uniform as possible.

2.2.4.4 pH stability of TrAA9A and PaAA9E

To assess the pH stability of TrAA9A and PaAA9E 12.5 µM of enzyme was incubated for 6 h, 3 h, 2 h, 1 h, 30 min and 0 min at 25 ºC in buffers with pH 5 and 7 (25 mM Na-acetate and 25 mM Na-phosphate, respectively) before performing a 2,6 -DMP activity assay. Included in the incubation were three controls: buffer, equimolar amount of enzyme boiled for 15 min, and 12.5 µM $CuSO_4$ in buffer.

2.2.5 Enzymatic hydrolysis of pre-treated spruce biomass

The dry weight of the pre-treated softwood biomass (provided by St1) was estimated by comparing the weights of biomass before and after 24 h incubation at 100 ºC. To mimic commercial enzymatic cocktails, a basic enzyme cocktail (BEC) consisting of three cellulases: 6 mg/g *T. reesei* cellobiohydrolase 1, 2mg/g *T. reesei* endoglucanase II, and 500 nkat/g *A. niger* β-glucosidase) was created prior to the assay. The hydrolytic efficiency of the BEC was measured on 50 mg/ml of biomass (dry weight), and to investigate whether PaAA9E or TrAA9A improved hydrolysis 2mg/g of each were added. Additionally, 2 mg/g of the TrAA3_2 growth supernatant was mixed with the BEC and TrAA9A to examine whether TrAA9A and TrAA3_2 acted synergistically. Mixtures of TrAA3_2 with the BEC, as well as TrAA9A with 2 mg/g bovine serum albumin (BSA) were used as control reactions. The reactions (see Table 1) were performed in a 0.2 M, pH 5.0 Na-acetate buffer,

which was heated to 45 ºC for 30 min at 150 rpm (Innova 44, Eppendorf™) before adding the enzymes. The reaction mixtures were then incubated for 4 and 24 h at 45 ºC, 200 rpm before collecting samples. The collected samples were incubated for 15 min at 98 ºC and centrifuged for 10 min, and the samples collected after 4 h were stored at -20 ºC until the 24 h samples were ready. The effect of an added reductant on the hydrolysis was assessed with an experiment where 0.7 mM H_2O_2 or 1 mM ascorbic acid was added to reactions 1, 2, and 7 (see Table 1).

Table 1. Enzymatic hydrolysis reactions

1	BEC*
2	BEC + TrAA9A
3	BEC + PaAA9E
4	BEC + TrAA3_2
5	BEC + TrAA3_2 + TrAA9A
6	BEC + TrAA9A + BSA
7	Buffer control

*Basic enzyme cocktail

6 mg/g *T. reesei* cellobiohydrolase (CBH1/Cel7A)

2 mg/g *T. reesei* endoglucanase (EGII/Cel5A)

500 nkat/g *A. niger* β-glucosidase (BGL/ Cel3A)

The amount of reducing sugars was quantified with the 3,5-dinitrobenzoic acid (DNS) method (Miller, 1959), which is commonly used for quantifying the hydrolysis of biomass samples. Reducing sugars have a free aldehyde or ketone group (HC=O or RC=O) and therefore monosaccharides, such as glucose, are reducing while di- or polysaccharides are not because the aldehyde/ketone groups are involved in the binding between monosaccharides. The reductant capabilities of these sugars mean that under alkaline conditions they are able to reduce DNS, inducing a change in absorbance. When lignocellulose is hydrolysed hemicellulose yields pentose sugars (xylose and arabinose) and cellulose yields glucose, and due to their reductant nature, the total amount of these sugars can be detected by an increase in absorbance at 540 nm as the colour of 3-amino,5-nitrosalicylic acid (reduced form of DNS) intensifies.

A glucose standard dilution series (2 g/L to 0.1 g/L) was prepared in ultrapure water. The samples were diluted 1:50 in ultrapure water, before boiling in 60% DNS for 5 min and cooling down in an ice bath. The absorbance was measured at 540 nm, and the amount of reducing sugars in the samples were calculated based on the glucose standard curve using Microsoft Excel.

3 RESULTS

3.1 Characterisation of TrAA3_2

Before this study the *T. reesei* genome had been analysed in an attempt to locate a cellobiose dehydrogenase (CDH) that might be coexpressed with LPMOs. However, it was discovered that although *T. reesei* contain ten genes encoding enzymes belonging to the AA3 family, it does not contain any gene encoding for a CDH. One of the ten AA3 genes had a signal sequence and this secreted enzyme was categorised as a member of the AA3_2 subfamily based on its amino acid sequence (work done by Nina Aro at VTT). In this work we expressed the TrAA3_2 and purified from the cultivation supernatant using ion-exchange chromatography. We were able to purify and concentrate to 0.129 mg/ml (V_{tot}=1 ml) TrAA3_2 from 2.5 ml supernatant using 1 ml columns, and 0.89 mg/ml (V_{tot}=1 ml) from 10 ml supernatant using 5 ml columns. The purity of TrAA3_2 was assessed with an SDS-PAGE analysis, the result of which can be seen in Figure 8. TrAA3_2 has a MW of 67 kDa, and the supernatant contained other proteins around 100, 55-50, 30, and 20 kDa. After purification TrAA3_2 produces the strongest band at 67 kDa, but faint bands can be seen at 100 kDa and just below TrAA3_2.

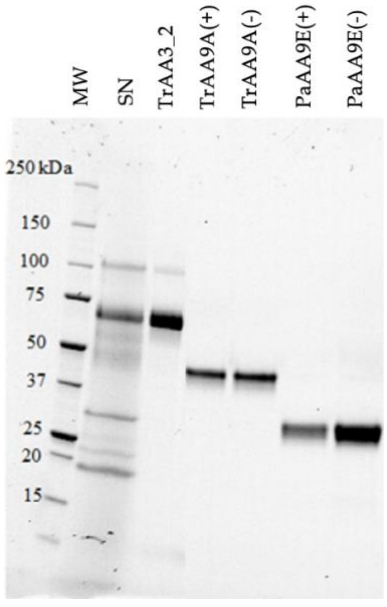

Figure 8 SDS-PAGE analysis of TrAA3_2 and the LPMOs TrAA9A and PaAA9E. SN stands for the TrAA3_2 supernatant, and (+) indicates the LPMO was copper-loaded, while (-) stands for the LPMO without copper-loading.

3.1.1 TrAA3_2 phylogenetic analysis

In order to analyse the phylogenetic relationship of TrAA3_2 to other AA3_2 family enzymes a sequence similarity network (SSN) was built using 2439 sequences as described by Sützl et al. (2019). The generated SSN represented in Figure 9 shows five phylogenetically distinct sequence clusters. The cluster were annotated based on the most frequently encountered enzyme type in each cluster to CDH (cellobiose dehydrogenases), AOx (alcohol oxidases), AAO-PDH (aryl-alcohol oxidases-pyranose dehydrogenases), GOx (glucose oxidases) and POx (pyranose oxidases). TrAA3_2 was found to be located in the GOx–cluster containing 103 glucose oxidases, 22 alcohol oxidases, 6 choline dehydrogenases, 5 glucose dehydrogenases, 2 cellobiose dehydrogenases, 1 amine oxidase, and TrAA3_2. The sequence identities within the cluster varied between 33.19 and 99.66 %.

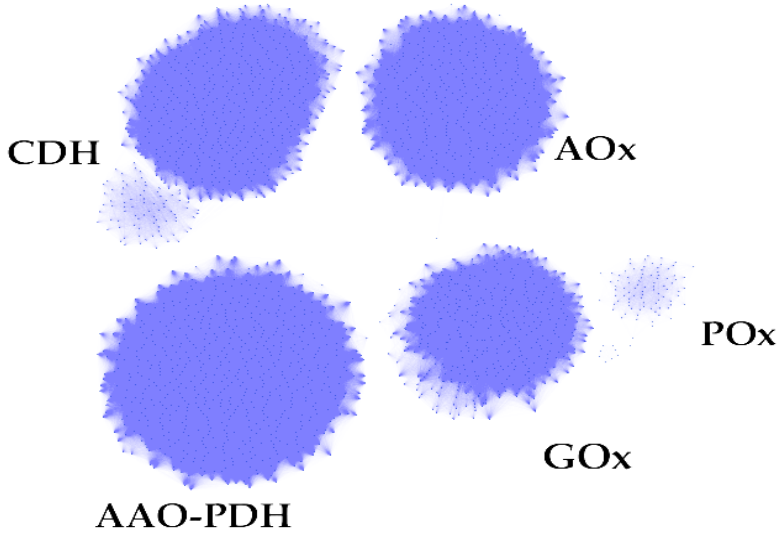

Figure 3 Sequence similarity network of AA3_2 family enzymes. The SSN was generated as described by Sützl et al. (2019) using 2439 sequences provided in their publication and the TrAA3_2 sequence. The clusters were annotated based on the most frequently encountered enzyme type in each cluster. TrAA3_2 was found in the GOx cluster.

3.2.2 TrAA3_2 activity

The AA3_2 –subfamily enzymes can broadly be divided to types that act on phenyl alcohols (which can be derived from lignin) or mono- and disaccharides (derived from hemicellulose/cellulose). Additionally, the oxidases of this subfamily can use O_2 as an electron acceptor and produce H_2O_2 in a concomitant reaction, while dehydrogenases require another electron acceptor. In this work, the activity of buffer-exchanged (20 mM Na-phosphate pH 6) TrAA3_2 supernatant was assayed with seven mono-or disaccharide and three phenyl alcohol substrates using five different assays. For the

LPMO-coupled assay purified TrAA3_2 was used. An overview including all substrates and positive controls can be found in Table 2.

Table 2. Overview of TrAA3_2 activity assays

Electron acceptor	Assayed substrates	Control enzymes	Assay
O_2	Veratryl alcohol, D-galactose, D-glucose, D-xylose, D-maltose, D-mannose, L-arabinose, D- (+)-cellobiose	Galactose oxidase (GAO) Glucose oxidase (GOx)	HRP-ABTS coupled LPMO –coupled 2,6-DMP assay FOx assay
Dichloroindophenol (DCIP)	Anisyl alcohol, Cinnamyl alcohol, Veratryl alcohol, D-glucose, D-galactose, L-arabinose, D- (+)-cellobiose, D-maltose	Aldose-aldose oxidoreductase (AAOR) Pyranose dehydrogenase (PDH)	DCIP-PMS assay
p-benzoquinone (BQ)	Anisyl alcohol, Cinnamyl alcohol, Veratryl alcohol, D-glucose, D- galactose	AAOR	BQ assay

Three different spectrophotometric oxidase assays were used in which molecular oxygen was acting as the electron acceptor. These were the coupled HRP-ABTS assay, the coupled 2,6-DMP LPMO assay and the ferric-xylenol orange assay. To confirm that the assays were working, *Dactylium dendroides* galactose oxidase and *A. niger* glucose oxidase were used as control enzymes. Although both sugar and phenyl alcohol substrates were tested, no activity could be detected with TrAA3_2. The results for the HRP-ABTS and DCIP -activity assays of TrAA3_2 displayed in Figure 10 A and B clearly illustrate the apparent inactivity of TrAA3_2. While the control reactions of AnGOx with 1-10 mM glucose led to an increase in product, TrAA3_2 barely generates any product even with 4 mM glucose (Figure 10 A).

As some AA3_2 enzymes prefer artificial electron acceptors over molecular oxygen, we also used two activity assays in which the artificial electron acceptors DCIP-PMS as well as p-benzoquinone were used. Three phenyl alcohols and several sugars were tested as substrates at concentrations up to 25 mM, and aldose-aldose oxidoreductase and pyranose dehydrogenase were used as control enzymes in the reactions. No activity could be detected for TrAA3_2 with any of the chosen substrates. As an example, the activity results for TrAA3_2 on anisyl and cinnamyl alcohol using the

DCIP-PMS assay are shown in Figure 10 B, which shows no decrease in the absorbance for the TrAA3_2 containing reactions. On the other hand, the control reaction with aldose-aldose oxidoreductase resulted in a clear decrease in absorbance when D-glucose was used as substrate.

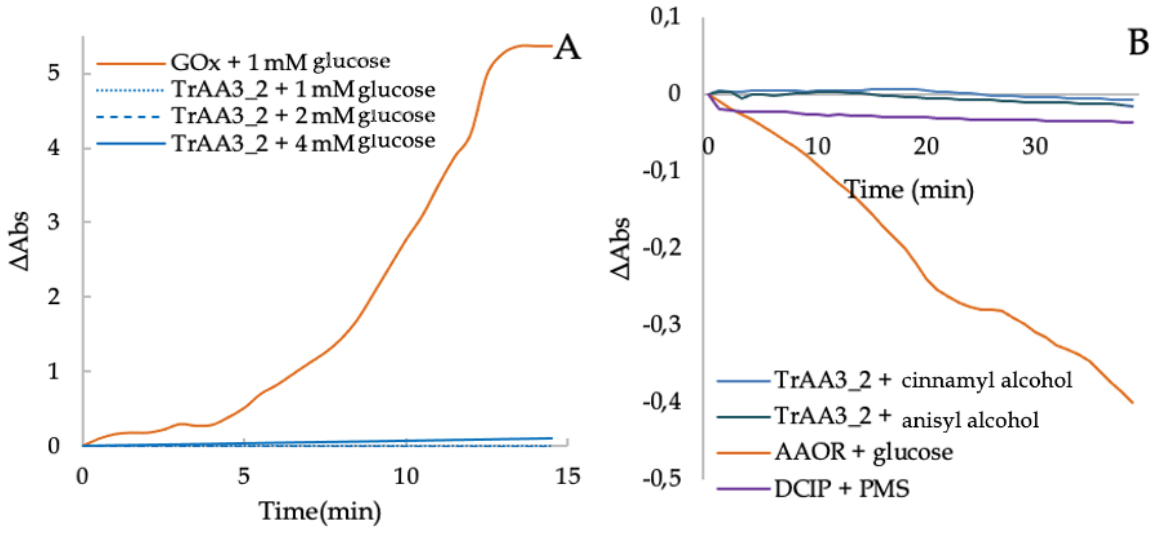

Figure 10 Activity of TrAA3_2 and AnGOx. (A) Activity of TrAA3_2 with AnGOx as control measured with an HRP-ABTS coupled assay using 0-4 mM glucose as the substrate. TrAA3_2 with 0 to 2 mM glucose does not show any activity, while TrAA3_2 with 4 mM glucose displays slight activity. GOx with 1 mM glucose is clearly active, while reactions with 2-4 mM glucose were too fast to observe. (B) Activity of TrAA3_2 with phenyl alcohols with aldose-aldose oxidoreductase as a control. The activity was measured with the DCIP-PMS assay using 10 mM of substrate with 25 µl TrAA3_2 supernatant or 0.8 µg aldose-aldose oxidoreductase in 250 µl reactions. TrAA3_2 is not displaying activity with cinnamyl or anisyl alcohol.

3.2.3 TrAA3_2 structural integrity

In order to analyse whether the FAD cofactor is incorporated into the TrAA3_2 enzyme, a UV-vis scan of purified enzyme was performed. Results from the FAD –cofactor scan between 600 and 250 nm illustrated in Figure 11, show that the FAD containing control enzyme AnGOx have three clear absorbance peaks at 450, 375, and 280 nm, characteristic for FAD (Figure 12), whereas TrAA3_2 does not give clear peaks at 450 and 375 nm.

The fold of TrAA3_2 was compared with the known FAD containig glucose oxidase by CD analysis. Figure 12 A and B represent acquired CD-spectra for TrAA3_2 and AnGOx, respectively, measured

at RT (coloured) and at 87 ºC (grey). Both TrAA3_2 and GOx seem to have a mostly α-helical secondary structure, and the characteristic α-helix dips at 208 nm and 222nm, are present in both spectra. Both enzymes were denatured at 87 ºC and no refolding was observed (data not shown).

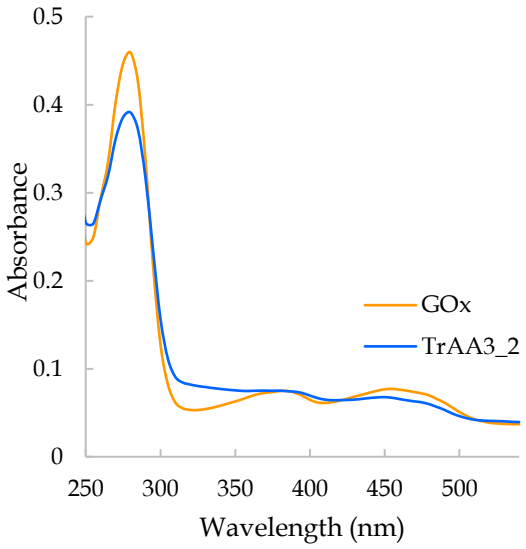

Figure 11 FAD-spectra of TrAA3_2 and AnGOx. Both enzymes display absorbance peaks around the characteristic FAD –peaks at 375 and 450 nm, but the TrAA3_2 peaks are less defined. The FAD –spectra were created by measuring the absorbance of 14 µM TrAA3_2 and 7 µM GOx in 20 mM Na-phosphate pH 6 between 250 and 550 nm with a 5 nm step size.

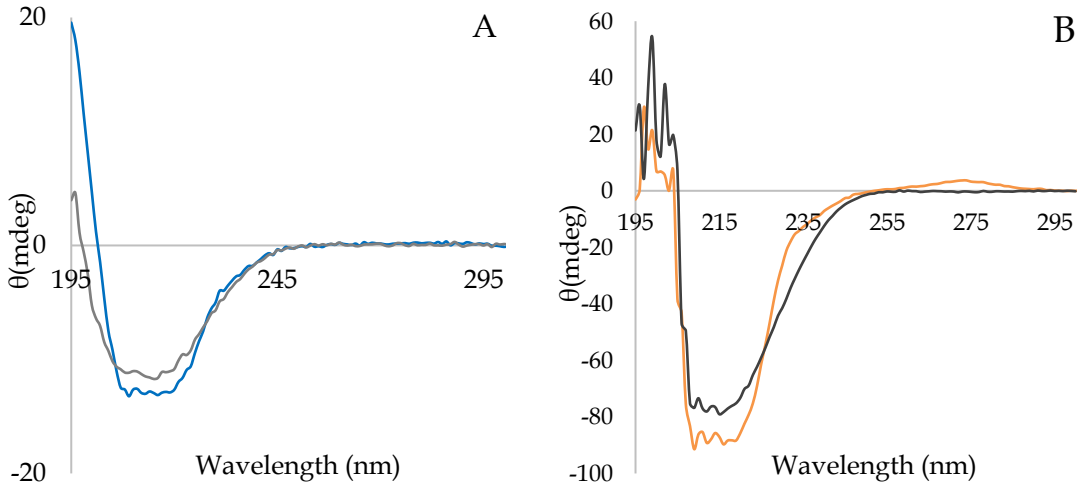

Figure 12 CD-spectra of TrAA3_2 and GOx. The degree of ellipticity was measured in 20 mM Na-phosphate pH 6 between 300 and 195 nm to compare the secondary structure content in TrAA3_2 and GOx and to observe the effect of heat on the spectra. **(A)** 3 µM TrAA3_2 native spectra at RT in blue and denatured spectra at 87 ºC in grey. **(B)** 31 µM GOx native spectra at RT in orange and denatured spectra at 87 ºC in grey.

3.1.3 TrAA3_2 homology model and structural analysis

A structural model of TrAA3_2 could be built based on the GDH from *Aspergillus flavus* glucose dehydrogenase (AfGDH, PDB ID: 4YNT), which in this structure is bound to D-glucono-1,5-lactone (the oxidation product of glucose by AfGDH). The sequence identity between AfGDH and TrAA3_2 was 41.6 %. The full homology model depicted in Figure 13 A reveals that TrAA3_2 has 9 alpha helices, and 2 β sheets. The quality estimates of the 3D model are included in Figure 13 D. The substrate-binding residues of TrAA3_2 and AfGDH are shown as space-filling spheres in Figure 13 B and as surface maps in figure 13 D. The figures show TrAA3_2 seems to have a less densely populated substrate-binding pocket than AnGOx. According to Yoshida et al (2015) the AfGDH forms hydrogen bonds with its substrate via His505 and His548, and the alignment with TrAA3_2 (Figure 13 C) reveals both of these are conserved in the TrAA3_2 sequence. As shown in Figure 13 C, AfGDH also interacts with its substrate with six other amino acids (Tyr53, Lys76, Gly413, Asn499, Arg501, Asn503), but only asparagine 503 is conserved in TrAA3_2. Additionally, in the *A. flavus* structure FAD is bound by residues Trp63, Thr89, Ala235, Phe504, and Ala538 (Yoshida et al. 2015). Out of these Ala235 and Phe504 are replaced in TrAA3_2 by Val258 and Ser527, respectively (not shown).

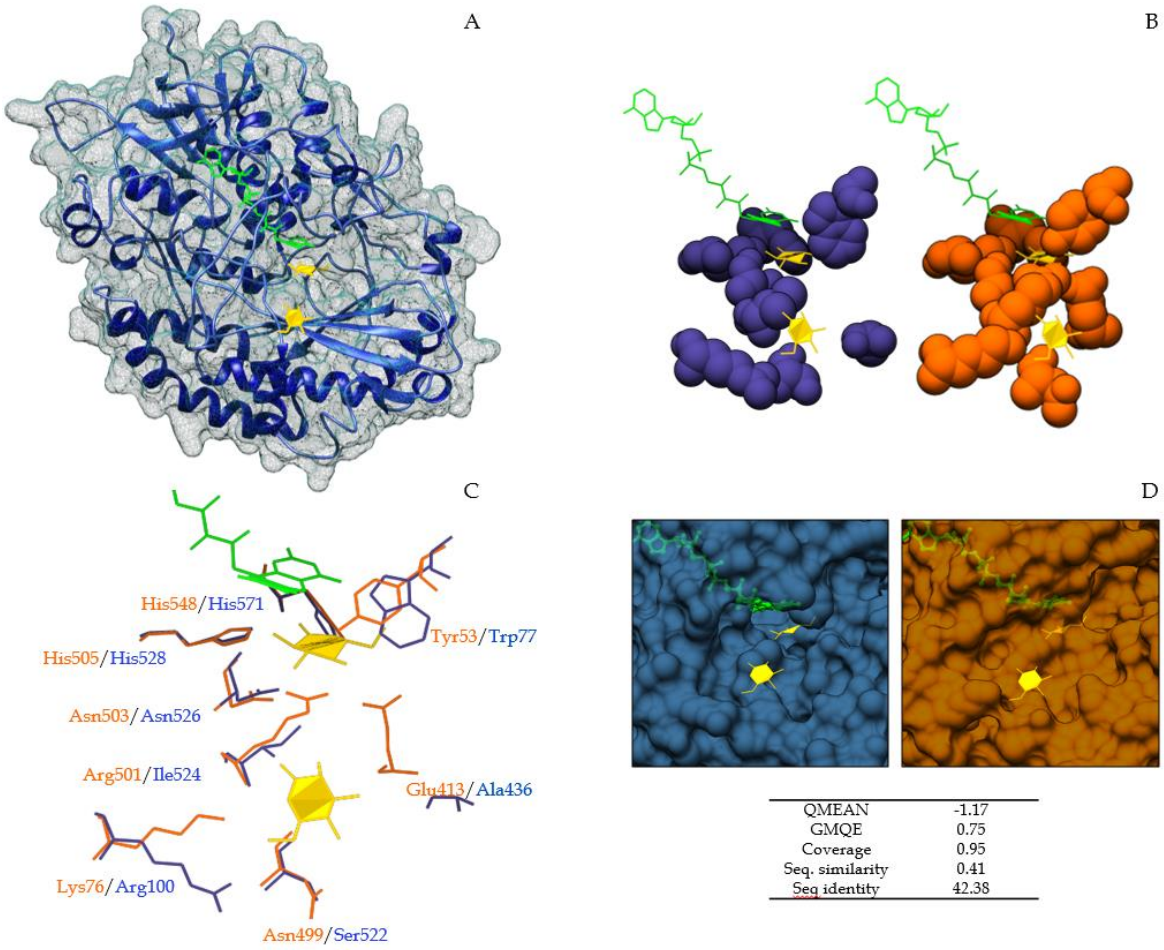

Figure 13 **TrAA3_2** homology model in comparison to 3D structure of AnGOx. **(A)** Homology model of TrAA3_2 built based on the crystal structure of AfGDH (PDB ID: 4YNT) with the SWISS-MODEL online tool **(B)** The substrate-binding pockets of TrAA3_2 (blue) and AnGOx (orange) with residue atoms depicted as space-filling spheres **(C)** Substrate-binding residues of **TrAA3_2** (blue) and AnGOx (orange) with the **FAD**-cofactor (green) and **product** (D-glucono-1,5-lactone) (yellow). **(D)** Surface models of FAD- and substrate-binding pockets of TrAA3_2 (blue) and AnGOx (orange) showing the FAD-cofactor in green and substrate in orange. The homology model was, AnGOx (PDB ID: 1CF3) was used as a comparison and the structures were compared with Chimera.

3.2 Characterisation of *Trichoderma reesei* TrAA9A and *Podospora anserina* PaAA9E

3.2.1 Effect of copper-loading and H_2O_2 sensitivity of TrAA9A and PaAA9E

Because LPMOs are copper-dependent enzymes and the copper is involved in the catalytic cycle we investigated whether copper-loading (i.e., incubating the LPMO with a 4x molar amount of copper

sulphate) had an impact on the activity of purified PaAA9E and TrAA9A. SDS-PAGE analysis of the purified, copper-loaded and unloaded, enzymes is shown in Figure 8. As is depicted in Figure 14, the activity of copper-loaded (+) TrAA9A is much higher than that of its unloaded (-) counterpart. Copper-loaded and unloaded PaAA9E, on the other hand, do not differ greatly from one another in their activity levels. Additionally, due to an ongoing debate of the true co-substrate of LPMOs (O_2 or H_2O_2), we assayed both copper-loaded and unloaded PaAA9E and TrAA9A in combination with varying concentrations of H_2O_2 to observe its effect on LPMO activity.

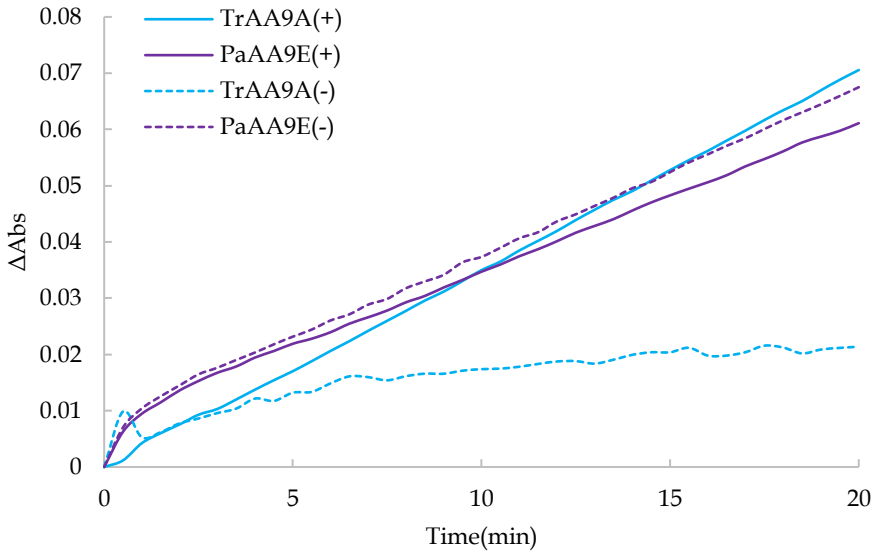

Figure 14 Effect of copper-loading on TrAA9A and PaAA9E. The copper-loaded (+) enzymes were incubated in 4 x molarity copper-sulphate before using the 2,6-DMP assay to compare their activity to unloaded (-) enzymes.

Copper-loaded (+) and unloaded (-) PaAA9E (Figure 15 A) are quite similar in their response to a growing H_2O_2 concentration as both increase in activity with the growing concentration up to 8 mM H_2O_2. At H_2O_2 concentrations higher than 2 mM, the activity of PaAA9E(-) appears slightly higher than its copper-loaded counterpart (maximum oxidation rates of 0.5 µM/min and 0.4 µM/min with 8 mM H_2O_2, respectively). While TrAA9A(+) oxidises 2,6-DMP at a much higher rate than its unloaded counterpart (3.6 µM/min vs. 0.8 µM/min with 2 mM H_2O_2), the activity of both TrAA9A(+) and TrAA9A(-) is enhanced by the addition of up to 2 mM H_2O_2 (Figure 15 B), and the activity starts decreasing at higher concentrations. Notably, the activity of TrAA9A (+) is still higher with 8 mM H_2O_2 compared to 1 mM H_2O_2. Overall, TrAA9A is impacted more by the addition of H_2O_2 than PaAA9E: the activity of TrAA9A rises rapidly with rising H_2O_2 concentrations up to 2 mM, but with higher concentrations of H_2O_2 its activity seems to be slightly inhibited. Additionally, TrAA9A seems more capable of oxidizing 2,6-DMP with an activity of 3.8 µM/min/mg with 2 mM H_2O_2, compared to 0.5 µM/min/mg for PaAA9E.

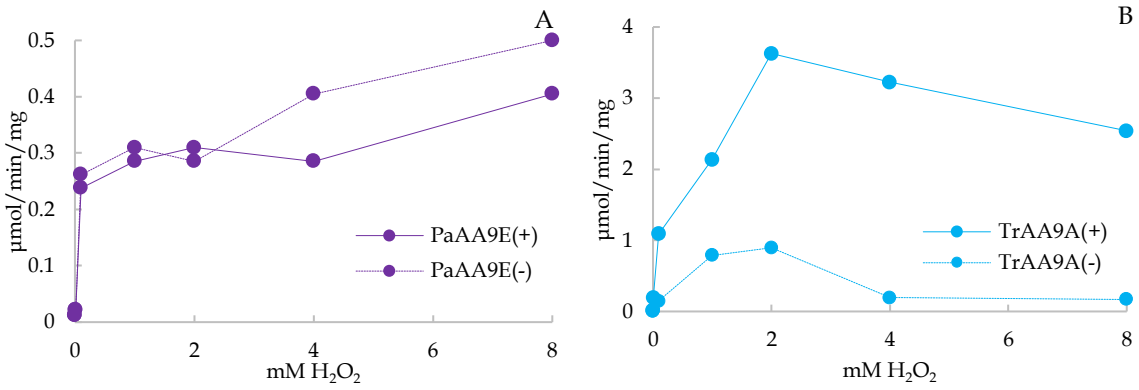

Figure 5 H_2O_2 dose-response curves for copper-loaded (+) and unloaded (-) PaAA9E and TrAA9A as activity for 2,6-DMP. **(A)** Both PaAA9E (+) and (-) show an increase in 2,6 –DMP oxidation as the amount of H_2O_2 increases. PaAA9E(-) reaches an oxidation rate of around 0.5 µM/min, while PaAA9E(+) reaches around 0.4 µM/min. **(B)** TrAA9A(+) is more efficient than TrAA9A(-) at oxidizing 2,6-DMP as it reaches an oxidation of around 3.6 µM/min while the rate for TrAA9A(-) remains below 1 µM/min. The rate of both starts decreasing with H_2O_2 concentrations above 2 mM. Activity was measured with the 2,6-DMP assay at 469 nm for 20 min using 1.25 µM enzyme and varying amounts of H_2O_2 (0, 0.01, 0.1, 1, 2, 4, and 8 mM). PaAA9E (+) and TrAA9A (+) were incubated with 4 x molarity copper for 30 min before the excess copper was removed.

3.2.2 Thermal and pH -stability of TrAA9A and PaAA9E

To study the thermal and pH -stability of TrAA9A and PaAA9E they were incubated at 40, 60, and 70 °C for up to 24 h, and at pH 5 and 7 for up to 6 h. The results are illustrated as percent activity in Figure 16. Both LPMOs retain their activity after incubation at 40 °C for 24 h and start losing their activity after just 30 min at 60 °C and 70 °C (Figure 16 A & B). As visualised in Figure 16 A, PaAA9E loses 90 and 99.5% of its activity after 24 h of incubation at 60 and 70 °C respectively, while Figure 16 B shows that TrAA9A retains 47 % of its activity after 24 h incubation at 60 °C, but loses 98% of activity after 24 h at 70 °C. Both PaAA9E and TrAA9A seem to be stable at pH 5 (Figure 16 C and D) up to 6 h, TrAA9A loses 5 % of its activity at pH 7 (Figure 16 D). The activity of TrAA9A seems to increase after 3 and 1 h at 40 and 60 C, respectively, and after 30 min at pH 5 and 7.

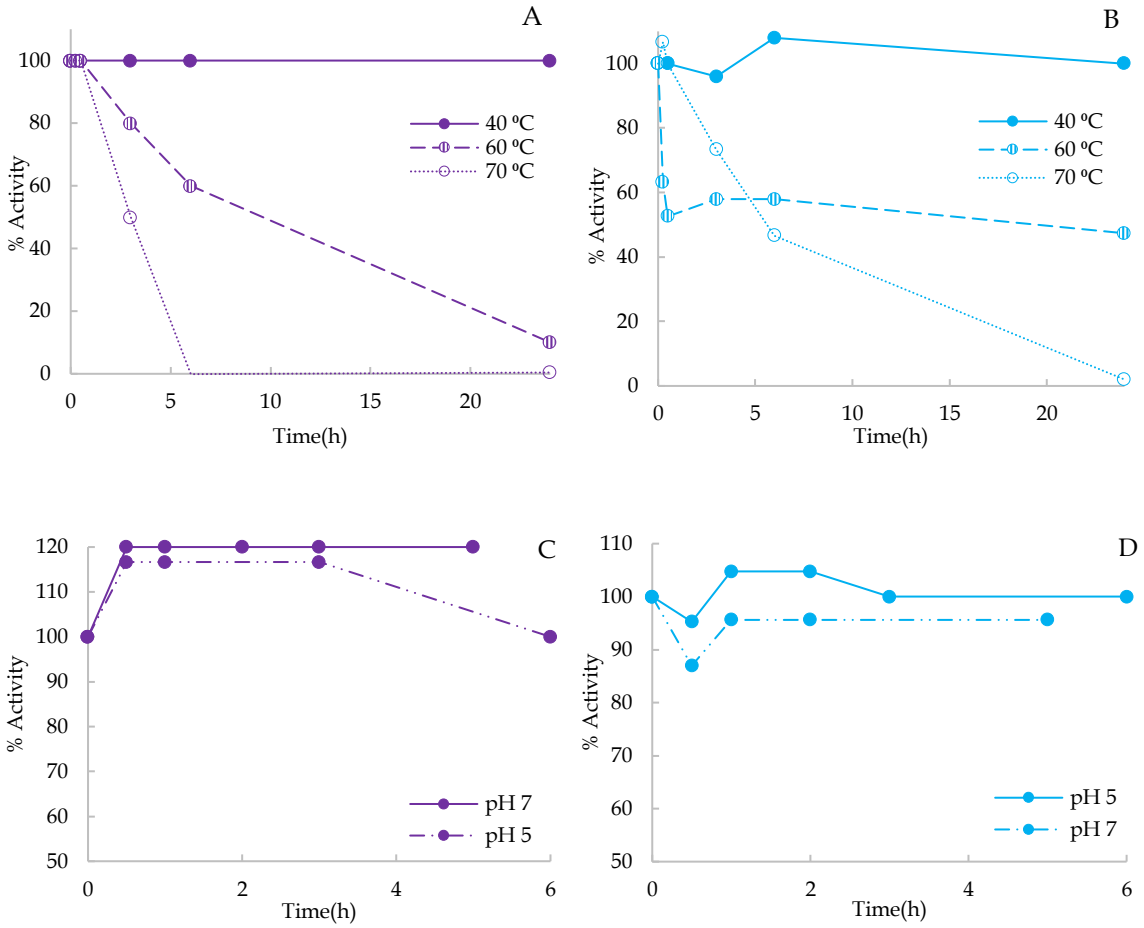

Figure 16 Thermal and pH stability of PaAA9E and TrAA9A **(A)** Thermal stability of PaAA9E at 40-70 ºC **(B)** Thermal stability of TrAA9A at 40-70 ºC **(C)** Stability of PaAA9E at pH 5 and 7 **(D)** Stability of TrAA9A at pH 5 and 7. Thermal stability was assessed by incubating the enzymes at 40, 60 and 70 ºC for 0 to 24 h in 25 mM Na-phosphate pH 6 and then performing a 2,6-DMP activity assay. The pH stability was measured by incubating the LPMOs in 25 mM Na-acetate pH 5 or Na-phosphate pH 7 for 6 and 5 hours, respectively, and then assaying 2,6-DMP oxidation.

3.3 Effect of TrAA9A, PaAA9E and TrAA3_2 on hydrolytic efficiency of pre-treated spruce biomass

We measured the hydrolytic efficiency of a cellulase mixture (referred to here as BEC) combined with TrAA9A, PaAA9A, and the TrAA3_2 growth supernatant to see how the addition of these LPMOs affects the hydrolysis, and whether TrAA3_2 is able to act synergistically with TrAA9A. Additionally, we performed an experiment with cellulases + TrAA9A in combination with H_2O_2 or ascorbic acid to investigate whether their addition is beneficial to the hydrolytic efficiency. The hydrolytic efficiency was quantified with the DNS-assay as the amount of reducing sugars.

Figure 17 depicts the hydrolytic efficiency of the cellulases alone and with various combinations of the studied LPMOs and TrAA3_2 as amount of reducing sugars measured after 4 h and 24 h. The hydrolysis experiments were done twice, and the results are presented separately (first repetition in Figure 17 A and C, and second repetition Figure 17 B and D). The cellulase mixture by itself (BEC) produced 2-4 g/l and 5-6 g/l of reducing sugars in 4 h and 24 h, respectively (Figure 17 A and B). Compared to the cellulases on their own the highest increase in yield was achieved by a combination of TrAA9A alone and with BSA (Figure 17 A and B) at a maximum increase of around 6 g/L in reducing sugars after 24 h. Some variance is apparent between the repetitions of these reactions, as in the first repetitions after 24 h the yield was 8 and 12 g/l for TrAA9A, and TrAA9A with BSA. PaAA9E does not seem to have had any effect on hydrolytic efficiency, as the amount of reducing sugars is nearly equivalent to the amounts in the BEC sample (Figure 17 A). Figures 17 C and D illustrate the results for adding H_2O_2 or ascorbic acid to the cellulase mixture with and without TrAA9A. There is some variance between the two repetitions of these reactions: in the first repetition the yield with added ascorbic acid was 5 and 13 g/l after 4 and 24 h, respectively, whereas in the second repetition the respective yields were 6 and 19 g/l. With added H_2O_2 we measured 6 and 12 g/l and 4 and 20 g/l after 4 and 24 h in the two repetitions. Figure 17 E depicts the impact of the TrAA3_2 supernatant on hydrolysis reactions with the cellulases and with TrAA9A. Compared to the yield of 6 g/L of reducing sugars of the cellulases by themselves, the addition of only the TrAA3_2 supernatant increased the yield by 5 g/L, whereas TrAA9A in combination with TrAA3_2 increased the yield only by 2 g/L.

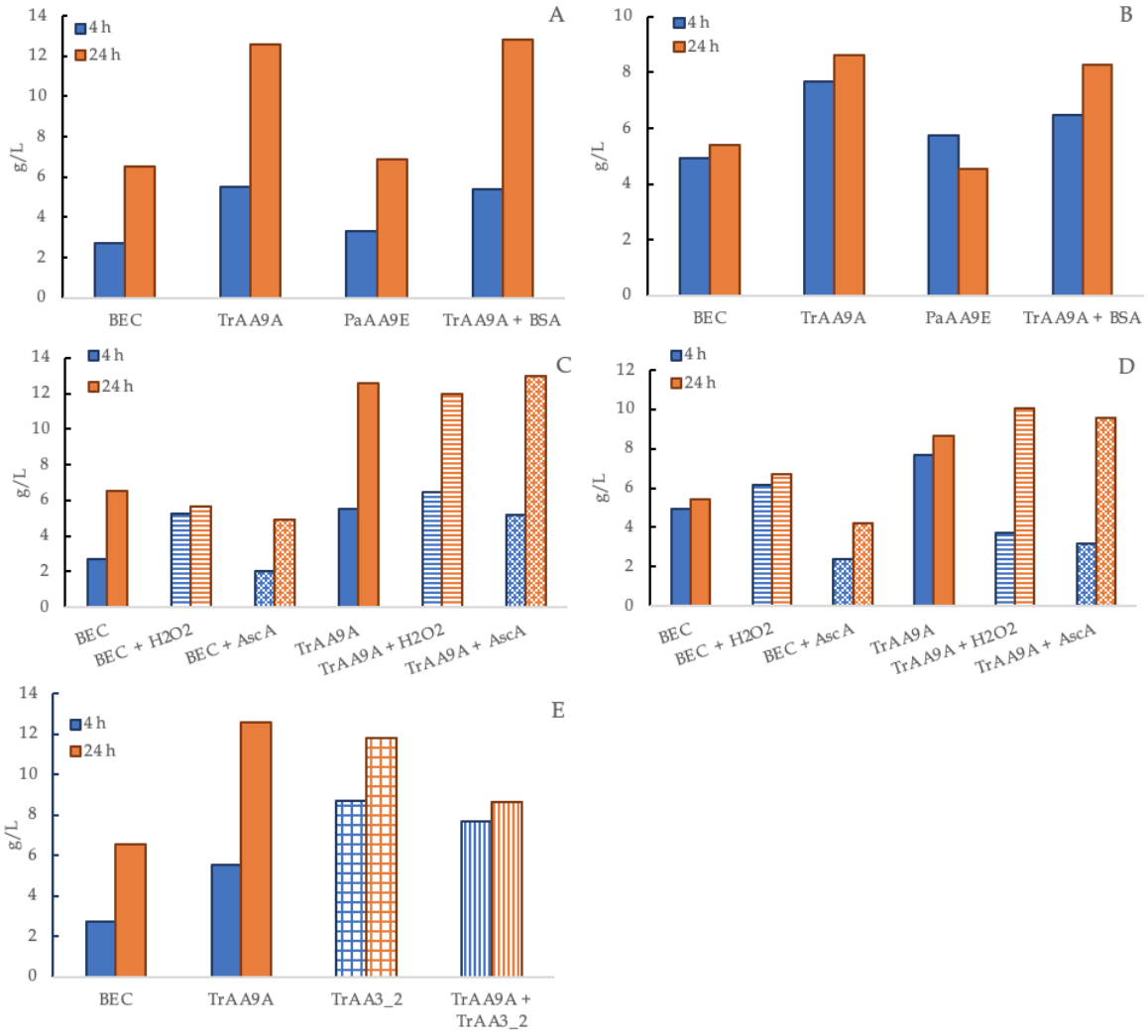

Figure 17 Effect of PaAA9E, TrAA9A, and TrAA3_2 on hydrolytic efficiency. The assay was repeated twice with the DNS-method. (**A)and (B)** Reducing sugars hydrolysed by a cellulase mixture in combination with TrAA9A and PaAA9E after 4 and 24 h in two repetitions. The cellulases (BEC) produce 5-6 g/l of reducing sugars in 24 h. TrAA9A with and without TrAA3_2 improves the hydrolytic efficiency of the cellulases, whereas PaAA9E has no effect. (**C) and (D)** The cellulase mixture (BEC) alone and with TrAA9A with 1 mM ascorbic acid. Reactions of BEC with added ascorbic acid yielded a comparable amount of reducing sugars as BEC without added ascorbic acid at 5-8 and 5-6 g/l respectively. TrAA9A with ascorbic acid produced 13 and 19 g/l reducing sugars in 24 h. The cellulases and TrAA9A without H_2O_2 produce 13 and 9 g/l reducing sugars in 24 h, and 12 and 10 g/l with added H_2O_2. (**E)** Effect of TrAA3_2 on hydrolytic efficiency. The addition of TrAA3_2 to BEC results in a roughly 6g/l increase in reducing sugars in 24 h, but only to a roughly 2 g/l increase when combined with the BEC and TrAA9A.

4 DISCUSSION

The process of degrading lignocellulosic biomass is yet to be fully understood, due to the complex network of organisms that are involved. Characterising the enzymes involved in this process is integral in order to understanding it and enabling the development of new applications. In this project we studied a novel AA3_2 family enzyme from *T. reesei*, as well as two LPMOs, from *T. reesei* and *P. anserina*, from the AA9 -family. We began by assaying the activity of TrAA3_2 and by analysing its phylogenetic relationship to other AA3_2 family members. After being unable to measure the activity of TrAA3_2 and identifying its closest neighbours as glucose oxidases, we examined whether the enzyme was folded properly and whether its FAD-cofactor was intact. We then turned our focus to TrAA9A and PaAA9A and found that copper-loading and using H_2O_2 as a cosubstrate may greatly alter their activity. Furthermore, we assessed their pH and thermal stability and found that both TrAA9A and PaAA9E are stable at the pH 5-7 and at 40 ^{o}C. Lastly, we performed hydrolysis experiments with a cellulase mixture in combination with TrAA9A, PaAA9E, and TrAA3_2, as well as H_2O_2 and ascorbic acid. We found that while PaAA9E has no effect on the hydrolytic efficiency, TrAA9A in combination with the TrAA3_2 supernatant, ascorbic acid or H_2O_2 seem to improve the hydrolytic efficiency of the cellulases.

4.1 Characterization of TrAA3_2

Some AA3_2 family enzymes have been shown to improve the activity of LPMOs, possibly by providing them with H_2O_2 (review Bissaro et al. 2018). Therefore, we aimed to characterise a novel TrAA3_2 enzyme that had been identified in a sequence analysis of *T. reesei* prior to this project. TrAA3_2 was assayed with various alcohol and carbohydrate substrates, as well as different electron acceptors in an attempt to account for the known variability of substrate and electron acceptor preferences of AA3_2 enzymes (reviewed by Sützl et al. 2018, compiled in CAZypedia, Lombard et al. 2013).

Because AA3_2's are yet to be characterised in detail (with only 10 listed as characterised in the CAZY database, http://www.cazy.org/AA3.html), it can be difficult to identify their substrate and conclusively determine whether they are active. We were unable to detect activity for TrAA3_2 with the chosen benzyl alcohols (veratryl alcohol, anisyl alcohol, and cinnamyl alcohol) and mono- and disaccharides (arabinose, cellobiose, galactose, glucose, maltose, mannose, and xylose) in combination with O_2 or quinone electron acceptors, even though phylogenetically TrAA3_2 is

similar to other AA3_2 enzymes, notably GOx's (Figure 9). While these results might mean that TrAA3_2 is inactive, it could also be that we were unable to find the correct substrate-electron acceptor combination, as all substrates were not assayed with all electron acceptors.

Because we were unable to find a suitable substrate and electron acceptor for TrAA3_2, we turned our attention to the structural aspects of TrAA3_2 to see whether it would offer an explanation for the apparent inactivity. AA3_2 enzymes contain an FAD-cofactor, integral to their activity (Sützl et al. 2018), which absorbs light at around 450 and 360 nm (Delfino et al. 2017). Therefore, if TrAA3_2 was fully intact, a spectrophotometric scan of the enzyme would result in clear peaks around these wavelengths. The poorly defined FAD peaks of TrAA3_2 shown in Figure 11 could mean a part of the enzymes are lacking FAD, which could explain why measuring TrAA3_2 activity remained unsuccessful. Because the absorbance spectrum of FAD is affected by both its state (reduced/oxidised) and its environment (i.e., the residues and solvent molecules surrounding it) (Delfino et al. 2017) the difference between TrAA3_2 and AnGOx –bound FAD absorbance peaks might also be due to this. Most of the FAD-binding residues are conserved in the TrAA3_2 structure based on the sequence alignment but based on the homology model shown in Figure 13 the residues in the TrAA3_2 FAD-binding pocket are less tightly packed than those of AfGDH, which could have an impact on the correct binding of FAD. However, because the homology structure is not of great quality any assessment of the conformational details is difficult.

The CD-spectra of TrAA3_2 and AnGOx measured at RT have a similar overall shape indicative of α-helical conformation, despite the tenfold concentration of AnGOx. However, some differences between the two spectra are apparent. A purely α-helical spectrum has two characteristic dips at 208 and 222 nm (source), which are well defined in the AnGOx spectrum (Figure 12 B), but not in the TrAA3_2 spectrum (Figure 12 A). The lack of clear dips may be due to the into low concentration, the structure, or perhaps a heterogeneous mixture of folded and unfolded TrAA3_2. The homology model of TrAA3_2 (Figure 13 A) shows that α-helices are prominent in the structure, but β-strands and -sheets are also present in the structure, corroborating the overall CD-spectrum

The homology model shown in Figure 13 shows that few of the substrate-binding residues of AfGDH are conserved in the TrAA3_2 structure. The residues forming hydrogen bonds with D-glucono-1,5-lactone (the product from glucose oxidation), in AfGDH (Lys76 and Asn 499) are replaced by Arg100 and Ser522, and the substrate-binding pocket seems to be tucked away (Figure 13 D). Both of these factors could negatively affect the affinity for carbohydrate substrates, and partially explain why we were unable to detect any activity on D-glucose, or other assayed

carbohydrate substrates. In contrast to the low similarity of substrate-binding residues between TrAA3_2 and AfGDH, Yoshida et al. (2015) stated that all but one (Glu413) of the substrate-binding residues found in AfGDH are conserved in the AnGOx structure. The active sites of these known glucose-active enzymes, AfGDH and AnGOx, are structurally more similar to one another than the TrAA3_2 active site, which might explain why TrAA3_2 displays hardly any activity even though phylogenetically it is close to GOx's. The substrate-binding site of TrAA3_2 might be an anomaly within the AA3_2 GOx structures, or it might be more suited for another type of substrate, which would make it a different type of enzyme. As the addition of the TrAA3_2 supernatant to the hydrolysis experiment resulted in an improvement in the overall yield, the possibility of another native substrate instead of glucose cannot be excluded, but the hydrolysis experiment would have to be repeated with purified TrAA3_2 to see whether the activity observed here was due to TrAA3_2 or another component in the supernatant. We assayed several alcohols and monosaccharides (Table 2) but were unable to find the correct substrate/assay. The pre-treated biomass likely contains some residual phenol compounds, as well as mono- and oligosaccharides in addition to the main component - cellulose. Theoretically, any of these could be a substrate for TrAA3_2, but if TrAA3_2 used monosaccharides it would likely not increase the rate of hydrolysis much (or rather the detectable thing i.e., reducing monosaccharides) as it would be consuming the end product.

4.2 Characterisation and comparison of TrAA9A and PaAA9E

The main reason LPMOs are researched so vigorously is that adding them to enzyme cocktails can significantly boost cellulase activity, and therefore improve the overall hydrolytic efficiency (Harris et al. 2010; Phillips et al. 2011). LPMO activity may be further enhanced by adding H_2O_2, small reductants such as ascorbic acid, or other secreted CAZymes such as cellobiose dehydrogenase or AA3 -family enzymes, which may be able to supply H_2O_2 (Phillips et al. 2011; Garajova et al. 2016; Kracher et al. 2016; Bissaro et al. 2018). Oxygen was originally thought to be the natural cosubstrate of LPMOs (Vaaje-Kolstad et al. 2010; Beeson et al. 2012) but in recent years more research suggests that the cosubstrate might be H_2O_2 instead, which calls into question the classification of these enzymes as oxygenases (Bissaro et al. 2017; Hegnar et al. 2019). The relationship between H_2O_2 and LPMOs is somewhat convoluted: on the one hand, LPMOs can produce H_2O_2 when not bound to their substrate (Kittl et al. 2012), but on the other hand providing LPMOs with H_2O_2 enhances their activity (Bissaro et al. 2017). H_2O_2 can drive LPMO activity after a so-called priming reaction, where the active site copper is reduced. H_2O_2 is then able to fuel several catalytic cycles before the copper needs to be reduced again, unlike in the O_2 driven reaction where the copper needs to be reduced at the beginning of each catalytic cycle (Bissaro et al. 2017). In 2017 Bissaro et al. argued that because

H_2O_2 could deliver the protons, electrons and oxygen required for hydrolysing the substrate, it is conceivable that H_2O_2 is the preferred co-substrate rather than O_2. And indeed, they found that LPMO activity was enhanced up to 26-fold when supplied with H_2O_2. Several groups have reached similar conclusions since then (Kuusk et al. 2018; Breslmayr et al. 2018; Hangasky et al. 2018), but the role of H_2O_2 with respect to the LPMO reaction and lignocellulose hydrolysis is not fully understood.

4.2.1 The 2,6-DMP assay as a tool to assay LPMO activity

The 2,6-DMP assay for LPMO enzymes relies on the ability of LPMOs to oxidize 2,6-DMP in the presence of hydrogen peroxide (Breslmayr et al. 2018). It is a great tool for LPMO research due to its sensitivity and was used successfully to determine the thermal and pH stability, as well as the effect of copper-loading and H_2O_2 addition on TrAA9A and PaAA9E. However, we did encounter significant activity of boiled LPMOs with added H_2O_2, which only disappeared after boiling the enzymes for an hour, which made analysing some of the results more difficult. Initially, we dismissed this as background activity possibly caused by excessive amounts of copper released as the enzymes denature or a reaction of 2,6-DMP with another component of the reaction mixture. However, after noticing that the boiled LPMOs can appear more active than their unboiled counterparts and that boiling the LPMOs for a full hour effectively removes the activity, it became clear that the causes are more complex. It may be that the structure of PaAA9E and TrAA9A allow them to retain some activity even in a partially denatured state. Disulphide bridges near the active site could account for this (Siddiqui et al. 2005; Yin et al. 2015) by protecting the copper active site. The TrAA9A structure (PDB ID: 5O2X) has two disulphide bridges located between res 56 – 177 and 97 – 101, which are not closely related to the active site. The background activity was difficult to eliminate, because there are several steps to the reaction mechanism that make it difficult to identify the source and differentiate between background activity and actual activity. Recently Bissaro et al published an improved 2,6-DMP assay method in which hydrocoerulignone is used as a starting point (effectively removing one reaction step). Due to time constraints, we were unable to repeat the experiments with hydrocoerulignone and thus we can only speculate whether the activity observed with the boiled LPMOs was residual activity or a background effect.

4.2.2 Characterisation of TrAA9A and PaAA9E stability and H_2O_2 dependent activity

Because LPMOs require a copper cofactor to function but the copper is surface-exposed, it is crucial to ensure that the majority of enzymes have bound copper before any further experiments. We

incubated TrAA9A and PaAA9E with 4 x molarity copper sulphate, and assayed copper-loaded LPMOs with unloaded equivalents to be able to measure and illustrate the effect of copper-loading after the enzymes had been stored at -20 ºC for up to a year. As is illustrated in Figures 14 and 15, PaAA9E and TrAA9A both displayed an increase in activity towards 2,6-DMP after copper loading, but the change was especially drastic for TrAA9A, because copper-loaded TrAA9A showed a 4-fold increase in activity compared to unloaded TrAA9A with 2 mM H_2O_2, while copper-loaded PaAA9E was only slightly more active than its unloaded counterpart with 0-2 mM H_2O_2, and less active with larger H_2O_2 concentrations, which suggests that TrAA9A is more prone than PaAA9E to losing its copper when stored at – 20 ºC for prolonged periods of time. However, the results obtained here do not reveal how quickly the copper detaches from TrAA9A, which might also have important implications for practical applications: if the copper detaches quickly it might hinder the use of TrAA9A as continuously reloading the enzyme with copper could raise costs or processing times significantly. These results highlight the importance of ensuring that the LPMOs are correctly loaded with copper prior to experiments. However, it has been suggested that LPMOs can obtain sufficient amounts of copper from biomass (Eijsink et al. 2019), which suggests no copper-loading would be necessary if experiments are performed on biomass. The observation made here that adding H_2O_2 to LPMO reactions enhances the rate of 2,6-DMP oxidation of both TrAA9A and PaAA9E (Figure 15) supports the previously made notions that H_2O_2 is a more suitable co-substrate for some LPMOs than O_2 (Bissaro et al. 2018; Kuusk et al. 2018; Jones et al. 2020). In a recent study Jones et al. (2020) quantified the digestion of phosphoric acid-swollen cellulose (PASC) and found that the reaction of *Hypocrea jecorina* (anamorph of *T. reesei*) AA9A (HjAA9A) with 400 µM H_2O_2 is 1000-fold faster than with O_2. In the experiments presented here, the rate of 2,6-DMP oxidation with 2 mM H_2O_2 reached 3.6 and 0.5 µg/ml/min for TrAA9A and PaAA9E, respectively, translating to a 280-fold and a 34-fold increase in the reaction rate when compared to reactions with no added H_2O_2. Furthermore, the 2,6-DMP assay results indicate that PaAA9E and TrAA9A can cope with large amounts of H_2O_2 without becoming inactivated: the activity of PaAA9E and TrAA9A for 2,6 –DMP reached its peak with 8 mM and 2 mM added H_2O_2, respectively, reaching activity levels of 0.5 and 3.6 µg/ml/min (Figure 15). In the landmark study by Bissaro et al. (2017) the activity of *Streptomyces coelicolor* LPMO 10C increased up to 30-fold when H_2O_2 was added, but the enzyme started to inactivate with less than 250 µM H_2O_2 in the presence of 1 mM ascorbic acid. In contrast to this, we did not observe any inactivation of PaAA9E, and TrAA9A only started to inactivate with 2 mM H_2O_2.

The thermal and pH stability of LPMOs are integral for their use in practical applications and experiments where the enzyme is subjected to certain conditions for a prolonged period. Depending on the thermostability, different LPMOs may be suitable for different applications: some

fermentation processes are carried out below 42 ºC, whereas for example steam pre-treatment makes the processing temperature considerably higher (Souza et al. 2012). Some LPMOs function optimally at 50 ºC (Agrawal et al. 2020) but optimal temperature is measured within a narrow time frame and does not reveal how well the enzyme is suited for many practical applications, where the enzyme is required the enzyme to be stable over prolonged periods of time. Because this project aimed to increase knowledge about the applicability of TrAA9A and PaAA9E for industrial applications, we opted for measuring their thermal stability instead of their optimal temperature.

Similarly to other LPMOs PaAA9E and TrAA9A are both stable at 40 ºC, as they retain 100 % activity after a 24 h incubation (illustrated in Figure 16). TrAA9A and PaAA9E start losing their activity after 30 min incubation at 60 ºC and retain 47 and 10 % of their activity after 24 h, respectively (Figure 16 A). While TrAA9A seems more thermally stable than PaAA9E, as it is notably more active after 24 h at 60 ºC than PaAA9E, its activity reduces to 2 % after 24 h at 70 ºC. We did not assess the stability of PaAA9E and TrAA9A between 40 and 60 ºC, but *Thermoascus aurantiacus* and *Talaeomyces cellulolyticus* AA9A, which are also stable at 40 ºC, retain approximately 60 and 70 % of their activity after 8 h at 45 ºC (Zhang et al. 2019). The activity of TrAA9A decreased to around 50 % within the first hour of incubation at 60 ºC and barely any further loss of activity was observed within 24 h. This result seems to indicate there was some variability within the enzyme sample and could mean different conformations of TrAA9A were present. The results obtained here suggest that PaAA9E and TrAA9A remain stable between pH 5 and 7, and at 40 ºC, and that TrAA9A is thermally more stable than PaAA9E.

4.2.2 Effect of AA9 LPMOs on hydrolysis of lignocellulose

The suitability of TrAA9A and PaAA9E for further experiments and practical applications in biomass processing was assessed by evaluating their impact on the hydrolysis of pretreated biomass by a mixture of cellulases. The obtained results vary notably between the two repetitions of this experiment, which may be due to several factors. One explanatory factor may be the composition of the biomass. If the biomass was non-homogeneous with regard to the amount of reducing sugars or water variable amounts of cellulose may have been present for the enzymes to act upon. Another important factor to consider is the possibility of contamination, as for example in the second repetition the cellulases with PaAA9E (Figure 17 B) produced fewer reducing sugars in 24 h than in 4 h, which does not seem to make sense with how cellulases and LPMOs are thought to interact. Thirdly, there may have been mistakes made in preparing the hydrolysis reactions of DNS-assay

samples. Even though the results are variable, the general trends within them offer some insight into the impact of TrAA3_2, TrAA9A, and PaAA9E on biomass hydrolysis.

Our results suggest that like many LPMOS, TrAA9A by itself may improve the hydrolysis of softwood biomass, while PaAA9E does not offer a clear improvement: adding TrAA9A to the hydrolysis reaction doubled the yield in 24 h, whereas PaAA9E addition had no considerable effect on the yield (Figure 17 A and B). The improvements to hydrolysis that we observed with TrAA9A are consistent with studies where adding LPMOs to enzymatic cocktails has significantly enhanced the hydrolytic efficiency (Harris et al. 2010), while the results obtained with PaAA9E are inconsistent with this, which may be due to several factors. One possibility is that the biomass is unsuitable for PaAA9E: for example, Zhang et al (2019) found that the *Talaromyces cellulolyticus* AA9A improved hydrolysis by approximately 10 and 24 % on Avicel and delignified corncob residue, respectively, in 7 days when compared to a control with BSA. Therefore, it is conceivable that the increase in hydrolytic efficiency is markedly higher on other types of biomass. Another factor that could play a role is the cellulase mixture (BEC), because PaAA9E oxidises at C1, and the oxidation product is a reducing sugar, it may be that the cellulases were unable to take advantage of the chain ends that PaAA9E created.

In a previous study the *Hypocrea jecorina* AA9A showed increased activity on pure cellulose with added H_2O_2 (Jones et al. 2020), which is consistent with our observations both in the 2,6-DMP assays and in the hydrolysis experiment. However, in the hydrolysis experiment adding 0.7 mM H_2O_2 to reactions with TrAA9A (Figure 17 D) only amounted to a 1.16 –fold increase in product compared to reactions without H_2O_2 in 24 h. Interestingly, H_2O_2 seems to improve hydrolysis by the cellulases alone, indicating that it may interact with either one of the enzymes in the cellulase cocktail (BEC), or perhaps somehow modify the biomass in a way that makes it more accessible to these enzymes.

This apparent difference in how TrAA9A reacts to H_2O_2 may be partially explained by the differences in the experimental setup, and the nature of the substrate. In a comprehensive study on the co-substrate preference of a C4-oxidising LPMO9E from *Myceliophthora thermophila* (MtLPMO9E) the solubility and concentration of the substrate resulted in differences in co-substrate preferences, as well as different products (Hangasky et al. 2018). Furthermore, while they found the activity of MtLPMO9E alone to be significantly enhanced by added H_2O_2, they did not observe a similar effect when assaying a full fungal secretome, which parallels the results presented here. Hangasky et al. (2018) concluded this to mean that H_2O_2 is not a relevant co-substrate under conditions that mimic lignocellulose degradation in nature. While it is possible to draw a similar conclusion based on the

results presented here, other possibilities have to be ruled out conclusively before doing so, especially since the experimental procedures were different. For instance, H_2O_2 can also be generated non-enzymatically by reactive oxygen species, which are often present in biomass as a consequence of oxidase or semiquinone reactions (review Bissaro et al. 2018) or can be generated as a consequence of hydrothermal pre-treatments of the biomass (Kont et al. 2019), meaning sufficient amounts of H_2O_2 may be present in the biomass itself, making adding H_2O_2 unnecessary. Because we did not observe a notable increase in hydrolysis when adding H_2O_2 to cellulases with TrAA9A (Figure 17 C and D), and because the increase in activity for TrAA9A was significantly larger in the 2,6-DMP assay (Figure 15 B), it is possible that H_2O_2 is already being generated by the system non-enzymatically. It is also possible that LPMOs could build up H_2O_2 slowly when they are not bound to their substrate and then use it to fuel their rapid activity once a substrate is bound (Hegnar et al. 2019). Repeating the experiment with a competitive peroxygenase, such as HRP may shed some light on the role of H_2O_2 in this particular biomass hydrolysis. Similarly, supplying the cellulase-TrAA9A -reaction with ascorbic acid did not seem to significantly improve the hydrolytic efficiency (around 1 g/L improvement). Plant- and fungus derived phenols (Kracher et al. 2016), as well as lignin fragments (Cannella et al. 2012) act as LPMO-reductants, which may explain the apparent inability of ascorbic acid to increase the hydrolytic efficiency of cellulases with TrAA9A: the softwood biomass and cellulases together may have provided a sufficient amount of aromatic compounds to fuel TrAA9A activity.

AA3_2 family enzymes are one proposed natural source of H_2O_2 for LPMOs (Hegnar et al. 2019). We were unable to detect TrAA3_2 activity by itself (discussed in detail above) but decided to include it in the hydrolysis experiment in case there is a mechanism by which it improves LPMO activity that was overlooked when designing the assays. Indeed, TrAA3_2 seems to enhance the hydrolytic efficiency in combination with TrAA9A, which would indicate TrAA3_2 is able to generate a reductant for TrAA9A from a species in the reaction mixture. However, we did not purify TrAA3_2 from the cultivation supernatant for this experiment, and because adding only TrAA3_2 to the BEC also improved the hydrolysis, there may be another component contributing to the hydrolysis in the TrAA3_2 supernatant.

4 CONCLUSIONS

TrAA3_2 was putatively assigned as a GOx based on phylogenetic analysis. However, we did not detect any activity for TrAA3_2 in an assay with AnGOx as a positive control, whereas in a biomass hydrolysis experiment the TrAA3_2 supernatant seemed to enhance the hydrolytic efficiency of a cellulase mixture. These conflicting results mean further studies are required to understand the function and role of TrAA3_2 in biomass degradation.

TrAA9A and PaAA9E are able to use H_2O_2 as a co-substrate, oxidation of in 2,6-DMP. The TrAA9A responded to hydrogen peroxide more than Pa AA9E, and the hydrogen peroxide concentrations that could be applied were surprisingly high. The results from the thermal and pH stability assays presented here suggest that PaAA9E and TrAA9A can be suitable candidates for practical applications between pH 5 and 7, and at 40 ºC. However, only TrAA9A seems to significantly improve softwood biomass hydrolysis by a basic mixture of cellulolytic enzymes. Adding excess H_2O_2 or ascorbic acid did not significantly improve the hydrolysis of softwood biomass by the cellulase mixture in combination with TrAA9A.

ACKNOWLEDGEMENTS

This work was a part of the Academy of Finland's Flagship Programme under Projects No. 318890 and 318891 (Competence Center for Materials Bioeconomy, FinnCERES).

REFERENCES

Beeson W, Phillips C, Cate J & Marletta M. 2012. Oxidative cleavage of cellulose by fungal copper-dependent polysaccharide monooxygenases. *J Am Chem Soc*. 134(2):890-892. doi:10.1021/ja210657t

Bennati-Granier C, Garajova S, Champion C, Grisel S, Haon M, Zhou S, Fanuel M, Ropartz D, Rogniaux H, Gimbert I, Record E & Berrin J. 2015. Substrate specificity and regioselectivity of fungal AA9 lytic polysaccharide monooxygenases secreted by Podospora anserina. *Biotechnol Biofuels*. 8(1). doi:10.1186/s13068-015-0274-3

Bischof R, Ramoni J & Seiboth B. 2016. Cellulases and beyond: the first 70 years of the enzyme producer Trichoderma reesei. *Microb Cell Fact*. 15(1):106. doi:10.1186/s12934-016-0507-6

Bissaro B, Røhr Å, Müller G, Chylenski P, Skaugen M, Forsberg Z, Horn S, Vaaje-Kolstad G & Eijsink V. 2017. Oxidative cleavage of polysaccharides by monocopper enzymes depends on H_2O_2. *Nat Chem Biol*. 13(10):1123-1128.

Bissaro B, Várnai A, Røhr Å & Eijsink V. 2018. Oxidoreductases and reactive oxygen species in conversion of lignocellulosic biomass. *Microbiol Mol Biol Rev*. 82(4). doi:10.1128/mmbr.00029-18

Breslmayr E, Daly S, Požgajčić A,Chang H, Rezić T, Oostenbrink C & Ludwig R. 2019. Improved spectrophotometric assay for lytic polysaccharide monooxygenase. *Biotechnol Biofuels*. 12(1):283. doi:10.1186/s13068-019-1624-3

Breslmayr E, Hanžek M, Hanrahan A, Leitner C, Kittl R, Šantek B, oostenbrink C & Ludwig R. 2018. A fast and sensitive activity assay for lytic polysaccharide monooxygenase. *Biotechnol Biofuels*. 2018;11(1):79. doi:10.1186/s13068-018-1063-6

Bucekova M, Valachova I, Kohutova L, Prochazka E, Klaudiny J & Majtan J. 2014. Honeybee glucose oxidase - Its expression in honeybee workers and comparative analyses of its content and H_2O_2-mediated antibacterial activity in natural honeys. *Naturwissenschaften*. 101(8):661-670.

Cannella D, Hsieh CWC, Felby C & Jørgensen H. 2012. Production and effect of aldonic acids during enzymatic hydrolysis of lignocellulose at high dry matter content. *Biotechnol Biofuels*. 5(1):26. doi:10.1186/1754-6834-5-26

Champreda V, Mhuantong W, Lekakarn H, Bunterngsook B, Kanokratana P, Zhao X, Zhang F, Inoue H, Fujii T & Eurwilaichitr L. 2019. Designing cellulolytic enzyme systems for biorefinery: From nature to application. *J Biosci Bioeng*. 128(6):637-654.

Couturier M, Haon M, Coutinho PM, Henrissat B, Lesage-Meessen L & Berrin J. 2011. Podospora anserina hemicellulases potentiate the *Trichoderma reesei* secretome for saccharification of lignocellulosic biomass. *Appl Environ Microbiol*. 77(1):237-246.

Cragg S, Beckham G, Bruce N, Bugg T, Distel D, Dupree P, Etxabe A, Goodell B, Jellison J, McGeehan J, McQueen-Mason S, Schnorr K, Walton P, Watts J & Zimmer M. 2015. Lignocellulose degradation mechanisms across the Tree of Life. *Curr Opin Chem Biol*. 29:108-119.

Danneels B, Tanghe M & Desmet T. 2019. Structural features on the substrate-binding surface of fungal lytic polysaccharide monooxygenases determine their oxidative regioselectivity. *Biotechnol J*. 14(3). doi:10.1002/biot.201800211

Davies G & Sinnott M. 2008. Sorting the diverse: The sequence-based classifications of carbohydrate active enzymes. *Biochem (Lond)*. 30(4):26-32.

de Souza C, Costa D, Rodrigues M, dos Santos A, Lopes M, Abrantes A, dos Santos Costa P, Silveira W, Passos F & Fietto L. 2012. The influence of presaccharification, fermentation temperature and yeast strain on ethanol production from sugarcane bagasse. *Bioresour Technol*. 109:63-69.

Eijsink V, Petrovic D, Forsberg Z, Mekasha S, Røhr Å, Várnai A, Bissaro B & Vaaje-Kolstad G. 2019. On the functional characterization of lytic polysaccharide monooxygenases (LPMOs). *Biotechnol Biofuels*. 12(1). doi:10.1186/s13068-019-1392-0

Espagne E, Lespinet O, Malagnac F, Da Silva C, Jaillon O, Porcel B, Couloux A, Aury J, Ségurens B, Poulain J, Anthouard V, Grossetete S, Khalili H, Coppin E, Déquards-Chablat M, Picard M, Contamine V, Arnaise S, Bourdais A, Berteaux-Lecellier V, Gautheret D, de Vries R, Battaglia E, Coutinho P, Danchin E, Henrissat B, Khoury R, Sainsard-Chanet A, Boivin A, pinan-Lucarré B, Sellem C, Debuchy R, Wincker P, Weissenbach J & Silar P. 2008.The genome sequence of the model ascomycete fungus Podospora anserina. *Genome Biol*. 9(5). doi:10.1186/gb-2008-9-5-r77

Florencio C, Cunha F, Badino A, Farinas C, Ximenes E & Ladisch M. 2016. Secretome data from Trichoderma reesei and Aspergillus niger cultivated in submerged and sequential fermentation methods. *Data Br*. 8:588-598.

Frommhagen M, Westphal A, van Berkel W & Kabel M. 2018. Distinct substrate specificities and electron-donating systems of fungal lytic polysaccharide monooxygenases. *Front Microbiol*. 9. doi:10.3389/fmicb.2018.01080

Garajova S, Mathieu Y, Beccia M, Bennati-Granier C, Biaso F, Fanuel M, Ropartz D, Guigliarelli B, Record E, Rogniaux H, Henrissat B & Berrin J. 2016. Single domain flavoenzymes trigger lytic polysaccharide monooxygenases for oxidative degradation of cellulose. *Sci Rep*. 6(1):1-9. doi:10.1038/srep28276

Greenfield N. 2007. Using circular dichroism spectra to estimate protein secondary structure. *Nat Protoc*. 1(6):2876-2890.

Guo H, Chang Y & Lee D. 2018. Enzymatic saccharification of lignocellulosic biorefinery: Research focuses. *Bioresour Technol*. 252:198-215.

Hangasky J, Iavarone A & Marletta M. 2018. Reactivity of O_2 versus H_2O_2 with polysaccharide monooxygenases. *Proc Natl Acad Sci U S A*. 115(19):4915-4920.

Hansson H, Karkehabadi S, Mikkelsen N, Douglas N, Kim S, Lam A, Kaper T Kelemen B, Meier K, Jones S, Solomon E & Sandgren M. 2017. High-resolution structure of a lytic polysaccharide monooxygenase from *Hypocrea jecorina* reveals a predicted linker as an integral part of the catalytic domain. *J Biol Chem*. 292(46):19099-19109.

Harris P V., Welner D, McFarland K, Re E, Navarro Poulsen J, Brown K, Salbo R, Ding H, Vlasenko E, Merino S, Xu F, Cherry J, Larsen S & Lo Leggio L. 2010. Stimulation of lignocellulosic biomass hydrolysis by proteins of glycoside hydrolase family 61: Structure and function of a large, enigmatic family. *Biochemistry*. 49(15):3305-3316.

Hegnar O, Petrovic D, Bissaro B, Alfredsen G, Várnai A & Eijsink V. 2019. pH-Dependent Relationship between Catalytic Activity and Hydrogen Peroxide Production Shown via Characterization of a Lytic Polysaccharide Monooxygenase from *Gloeophyllum trabeum*. *Appl Environ Microbiol*. 85(5) doi:10.1128/AEM.02612-18

Jeske L, Placzek S, Schomburg I, Chang A & Schomburg D. 2019. BRENDA in 2019: a European ELIXIR core data resource. *Nucleic Acids Res*. 47: D542–D549. doi:10.1093/nar/gky1048

Jones S, Transue W, Meier K, Kelemen B & Solomon E. 2020.Kinetic analysis of amino acid radicals formed in H_2O_2-driven CuI LPMO reoxidation implicates dominant homolytic reactivity. *Proc Natl Acad Sci U S A*. 117(22). doi:10.1073/pnas.1922499117

Karlsson J, Siika-Aho M, Tenkanen M & Tjerneld F. 2002. Enzymatic properties of the low molecular mass endoglucanases Cel12A (EG III) and Cel45A (EG V) of Trichoderma reesei. *J Biotechnol*. 99(1):63-78.

Kelly S & Price N. 2005. The Use of Circular Dichroism in the Investigation of Protein Structure and Function. *Curr Protein Pept Sci*. 1(4):349-384.

Kittl R, Kracher D, Burgstaller D, Haltrich D & Ludwig R. 2012. Production of four Neurospora crassa lytic polysaccharide monooxygenases in Pichia pastoris monitored by a fluorimetric assay. Biotechnol Biofuels. 5(1)70. Doi: 10.1186/1754-6834-5-79.

Kont R, Pihlajaniemi V, Borisova A, Aro N, Marjamaa K, Loogen J, Büchs J, Eijsink V, Kruus K & Väljmäe P. 2019. The liquid fraction from hydrothermal pretreatment of wheat straw provides lytic polysaccharide monooxygenases with both electrons and H_2O_2 co-substrate. *Biotechnol Biofuels*. 12(1). doi:10.1186/s13068-019-1578-5

Kontturi E, Laaksonen P, Linder M, Nonappa, Gröschel A, Rojas O & Ikkala O. 2018. Advanced materials through assembly of nanocelluloses. *Adv Mater*. 30(24). doi:10.1002/adma.201703779

Kracher D, Scheiblbrandner S, Felice A,Breslmayr E, Preims M, Ludwicka K, Haltrich D, Eijsink V & Ludwig R. 2016. Extracellular electron transfer systems fuel cellulose oxidative degradation. Science. 352:1098-1101

Kujawa M, Volc J, Halada P, Sedmera P, Divne C, Sygmund C, Leitner C, Peterbauer C & Haltrich D. 2007. Properties of pyranose dehydrogenase purified from the litter-degrading fungus Agaricus xanthoderma. *FEBS J*. 274(3):879-894.

Kuusk S, Bissaro B, Kuusk P, Forsberg Z, Eijsink V, Sørlie M & Väljmäe P. 2018. Kinetics of H_2O_2-driven degradation of chitin by a bacterial lytic polysaccharide monooxygenase. *J Biol Chem*. 293(2):523-531.

Kuusk S, Kont R, Kuusk P, Heering A, Sørlie M, Bissaro B, Eijsink B & Väljmäe P. 2019. Kinetic insights into the role of the reductant in H_2O_2-driven degradation of chitin by a bacterial lytic polysaccharide monooxygenase. *J Biol Chem*. 294(5):1516-1528.

Lombard V, Golaconda Ramulu H, Drula E, Coutinho P & Henrissat B. 2014. Carbohydrate-active enzymes database (CAZy) in 2013. *Nucleic Acids Res*. 42(D490–D495). doi:10.1093/nar/gkt1178

Martinez D, Berka R, Henrissat B, Saloheimo M, Arvas M, Baker S, Chapman J, Chertkov O, Countinho P, Cullen D, Danchin E, Grigoriev I, Harris P, Jackson M, Kubicek C, Han C, Ho I, Larrondo L, De Leon A, Magnuson J, Merino S, Misra M, Nelson B, Putnam N, Robbertse B, Salamov A, Schmoll M, Terry A, Thayer M, Westerholm-Parvinen A, Schoch C, Yao J, Barbote R, Nelson M, Detter C, Bruce D, Kuske C, Xie G, Richardson P, Rokhsar D, Lucas S, Rubin E, Dunn-Coleman N, Ward M & Brettin T. 2008. Genome sequencing and analysis of the biomass-degrading fungus Trichoderma reesei (syn. Hypocrea jecorina). *Nat Biotechnol*. 26(5):553-560.

Mashayekhi Mazar F, Martinez J, Tyagi M, Alijanianzadeh M, Turner A & Jager E. 2019. Artificial muscles powered by glucose. *Adv Mater*. 31(32). doi:10.1002/adma.201901677

Mathieu Y, Piumi F, Valli R, Aramburu J, Ferreira P, Faulds C & Record E. 2016. Activities of secreted aryl alcohol quinone oxidoreductases from Pycnoporus cinnabarinus provide insights into fungal degradation of plant biomass. *Appl Environ Microbiol*. 82(8):2411-2423.

Miller GL. 1959. Use of dinitrosalicylic acid reagent for determination of reducing sugar. *Anal Chem*. 31(3):426-428.

Phillips C, Beeson W, Cate J & Marletta M. 2011. Cellobiose dehydrogenase and a copper-dependent polysaccharide monooxygenase potentiate cellulose degradation by Neurospora crassa. *ACS Chem Biol*. 6(12):1399-1406.

Ramasamy K, Kelley R & Reddy C. 1985. Lack of lignin degradation by glucose oxidase-negative mutants of *Phanerochaete chrysosporium*. *Biochem Biophys Res Commun*. 131(1):436-441.

Reese E, Siu R & Levinson H. 1950. The biological degradation of soluble cellulose derivatives and its relationship to the mechanism of cellulose hydrolysis. *J Bacteriol*. 59(4):485–497.

Sankaran R, Parra Cruz R, Pakalapati H, Show P, Ling T, Chen W & Tao Y. 2019. Recent advances in the pretreatment of microalgal and lignocellulosic biomass: A comprehensive review. *Bioresour Technol*. doi: 10.1016/J.BIORTECH.2019.122476

Siddiqui K, Poljak A, Guilhaus M, Feller G, D'Amico S, Gerday C & Cavicchioli R. 2005. Role of disulfide bridges in the activity and stability of a cold-active α-amylase. *J Bacteriol*. 187(17):6206-6212.

Silar P. 2013. Podospora anserina: From laboratory to biotechnology. In: *Genomics of soil- and plant-associated fungi*. Vol 36. Springer, Berlin, Heidelberg, pp.283-309.

Sützl L, Foley G, Gillam EMJ, Bodén M & Haltrich D. 2019. The GMC superfamily of oxidoreductases revisited: Analysis and evolution of fungal GMC oxidoreductases. *Biotechnol Biofuels*. (1). doi:10.1186/s13068-019-1457-0

Sützl L, Laurent C, Abrera A, Schütz G, Ludwig R & Haltrich D. 2018. Multiplicity of enzymatic functions in the CAZy AA3 family. *Appl Microbiol Biotechnol*. 102(6):2477-2492.

Tuck C, Pérez E, Horváth I, Sheldon R & Poliakoff M. 2012. Valorization of biomass: Deriving more value from waste. *Science*. 337(6095):695-699.

Tzanov T, Costa S, Gü Bitz B & Cavaco-Paulo A. 2002. Hydrogen peroxide generation with immobilized glucose oxidase for textile bleaching. *J.Biotec*. 93:87-94.

Urban L, Goodall D, Bergström E & Bruce N. 2006. 1,4-Benzoquinone-based electrophoretic assay for glucose oxidase. *Anal Biochem*. 359(1):35-39.

Vaaje-Kolstad G, Horn S, van Aalten D, Synstad B & Eijsink V. 2005. The non-catalytic chitin-binding protein CBO21 from Serratia marcescens is essential for chitin degradation. J Biol Chem. 280(31):28492-28497.

Vaaje-Kolstad G, Westereng B, Horn S, Liu Z, Zhai H, Sørlie M & Eijsink V. 2010. An oxidative enzyme boosting the enzymatic conversion of recalcitrant polysaccharides. *Science*. 330(6001):219-222.

Wang Y & Zhang B. 2013. Biochemical conversion of ethanol from lignocellulose. In: *Biomass Processing, Conversion, and Biorefinery*. Nova Science Publishers, Inc., pp. 348-366.

Wong C, Wong K & Chen X. 2008. Glucose oxidase: natural occurrence, function, properties and industrial applications. *Appl Microbiol Biotechnol*. 78(6):927-938.

Yin X, Hu D, Li J, He Y, Zhu T & Wu M. 2015. Contribution of disulfide bridges to the thermostability of a type A feruloyl esterase from Aspergillus usamii. *PLoS One*. 10(5). doi: 10.1371/journal.pone.0126864

Zabed H, Akter S, Yun J, Zhang G, Awad F, Qi X & Sahu J. 2019. Recent advances in biological pretreatment of microalgae and lignocellulosic biomass for biofuel production. *Renew Sustain Energy Rev*. 105:105-128.

Zhang R, Liu Y, Zhang Y, Feng D, Hou S, Guo W, Niu K, Jiang Y, Han L, Sindhu L & Fang X. 2019. Identification of a thermostable fungal lytic polysaccharide monooxygenase and

evaluation of its effect on lignocellulosic degradation. *Appl Microbiol Biotechnol*. 103(14):5739-5750